Quaternary Science Reviews 377 (2026) 109814

Contents lists available at ScienceDirect

Quaternary Science Reviews

journal homepage: www.elsevier.com/locate/quascirev

# Environmental changes in western Siberia over the past 1800 years reconstructed by geochemical and biological records of a well-dated core from Zolotoe Lake in Altai Krai, Russia

Eslam M.A. Mitwally [a,b,1], Gulnara Nigamatzyanova [c,1], Larisa Frolova [c,d,*], Tzu-Tsen Shen [a], Vera Strakhovenko [e], Andrei A. Andreev [f], Ya-Hsuan (Sophia) Liou [a], Hong-Chun Li [a,g,**]

[a] Department of Geosciences, National Taiwan University, Taipei, 106319, Taiwan, ROC
[b] Department of Geology, Faculty of Science, Al-Azhar University, Assiut, Egypt
[c] Institute of Archaeology & Ethnography, Russian Academy of Sciences, Siberian Branch, 15 Lavrentieva Ave., 17, Novosibirsk, 630090, Russia
[d] Department of Zoology and General Biology, Kazan (Volga Region) Federal University, Kazan, 420008, Russia
[e] Sobolev Institute of Geology and Mineralogy Siberian Branch Russian Academy of Sciences, Novosibirsk, 630090, Russia
[f] Alfred Wegener Institute for Polar and Marine Research, Potsdam, 14473, Germany
[g] Frontiers Science Center for Deep Ocean Multispheres and Earth System, Key Laboratory of Marine Chemistry Theory and Technology, Ministry of Education, Ocean University of China, Qingdao, China

ARTICLE INFO

Handling Editor: P Rioual

*Keywords:*
West Siberia
Lake sediment core
Late Holocene
Elemental geochemistry
Pollen
Mineralogy
Climate change

ABSTRACT

A 64-cm long sediment core from Zolotoe Lake (51°51′28.74″N, 80°15′59.16″E), situated in the Kulunda Plain in the West Siberian Lowland of Russia, has been dated with Accelerator Mass Spectrometry (AMS) $^{14}C$ (37 dates), $^{210}Pb$ and $^{137}Cs$ (upper 19 cm) methods, providing a continuous record since ca 1800 cal yr BP. The comparisons of paired $^{14}C$ ages of A- and ABA-treated sedimentary total organic carbon (TOC) from 20 horizons indicate that old carbon influence (OCI) existed on some ABA-treated samples due to uptake of dissolved $CO_2$ in the lake water. Combining sedimentary feature, mineralogy, geochemical proxies and pollen assemblages, we reconstructed detailed environmental changes since 200 CE. The acid-leachable (0.5N HCl, AL) elements and Aqua Regia open dissolution (AR) elements measured by ICP-OES were discussed for deciphering lake chemistry and terrestrial input. In the Zolotoe Lake core, AL Ca/K instead of Sr/Ca and Mg/Ca is an indicator of lake salinity, with higher ratio reflecting higher salinity; and vice versa. AL Al/Ti is positively correlated with surface runoff. AL Mn/Fe and Mn/Al (rather than AL U/Al) are proxies for redox conditions with higher ratio pointing more oxic conditions. During Roman Warm Period (RWP, 200-400 CE) warming and wet conditions were prevailing. Cold and wet climates occurred during Dark Ages Cold Period (DACP, 450-800 CE). Many lakes in the Volchikhinsky lake system might be connected at that time to form a large lake. During the Medieval Climate Anomaly (MCA, 900-1300 CE), warm and relatively wet conditions prevailed in the interval 900-1200 CE; but from 1200 to 1300 CE climate was warmer and drier. Colder and drier conditions coincided with the early Little Ice Age (LIA) (1400-1750 CE), but the late LIA (1750-1850 CE) climate was cold and wet. The large Volchikhinsky Lake became a lake system with separated small lakes around 1600 CE. The Current Warm Period (CWP, 1850 CE-present), warming trend is documented in the lake sediments coinciding well with regional instrumental records. The Zolotoe Lake sediments reflect strong human impact since 1950 CE.

* Corresponding author. Institute of Archaeology & Ethnography, Russian Academy of Sciences, Siberian Branch, 15 Lavrentieva Ave., 17, 630090, Novosibirsk, Russia.
** Corresponding author. Department of Geosciences, National Taiwan University, Taipei, 106319, Taiwan, ROC.
*E-mail addresses:* t107799401@ntut.org.tw (E.M.A. Mitwally), gulnaraniga@mail.ru (G. Nigamatzyanova), larissa.frolova@mail.ru (L. Frolova), ttshen@ntu.edu.tw (T.-T. Shen), strahova@igm.nsc.ru (V. Strakhovenko), aandreev@awi.de (A.A. Andreev), yhliou@ntu.edu.tw (Y.-H.(S. Liou), hcli1960@ntu.edu.tw (H.-C. Li).
[1] Shared first authors.

https://doi.org/10.1016/j.quascirev.2026.109814
Received 18 July 2025; Received in revised form 14 January 2026; Accepted 14 January 2026
Available online 10 February 2026

## 1. Introduction

Paleoclimate and paleoenvironmental changes during the Late Holocene in the Northern Hemisphere are very important information for evaluating the current global warming and its forcing factors. High-resolution multi-proxy records from well-dated lake sediments are essential for reconstructing such changes (Chappell, 1999; Smol and Cumming, 2000; Chen et al., 2006; Hausmann et al., 2011; Lan et al., 2018; Blyakharchuk et al., 2020; Misra et al., 2025). Although paleoenvironmental reconstructions based on lake records are rather abundant in southern Siberia (e.g., Blyakharchuk et al., 2004, 2007, 2008, 2017, 2020; Khazina, 2006; Andreev et al., 2007; Kalugin et al., 2007, 2013; Rudaya and Li, 2013; Rudaya et al., 2012, 2016; Ryabogina et al., 2019; Bezrukova et al., 2023, 2025; Misra et al., 2025), high-resolution reconstructions with reliable chronology are still limited. Information on climate and environmental conditions during the last 2000 years is critical for understanding the baseline of natural climate variability, contextualizing modern climate change, evaluating climate models, and understanding how human societies respond to environmental pressures (Wuebbles et al., 2017). For reconstruction of climate and environmental conditions over the past 2000 years using lake records in this vast territory, two major difficulties are often encountered: (1) lack of high-resolution AMS $^{14}C$ dating and (2) weak understanding of geochemical proxies in lake systems because of pretreatments and analytical methods of lake sediments. Scattered dating points in a sediment sequence not only result in large uncertainties in chronology of the lake records, but also obscure the reliability of $^{14}C$ dates affected by old carbon influence (OCI) because of dissolved $CO_2$ uptake from lake water and reworking events in sedimentary sequences (Shore et al., 1995). For instance, Blyakharchuk et al. (2020) published 48 AMS $^{14}C$ dates from an 82-cm core collected in the fresh Manzherok Lake in a forest–steppe zone on the western piedmonts of the Altai Mountains. Many $^{14}C$ dates of the rich TOC contained OCI due to uptake of dissolved $CO_2$ from the lake water. Those dissolved $CO_2$ might come from decomposition of old organic matters and $CH_4$ degassing. Therefore, a better chronological construction must exclude those OCI-effected $^{14}C$ dates. For saline lakes, $^{14}C$ dating is more problematic (Zhou et al., 2021). Misra et al. (2025) reported 35 AMS $^{14}C$ dates from a 30-cm gravity core retrieved from Shira Lake (Republic of Khakassia, Russia). Although the OCI effect from carbonates can be largely eliminated by acid treatment, many $^{14}C$ dates on TOC appeared significantly older due to uptake of dissolved $CO_2$ during the photosynthesis of organic carbon formation. In addition to the detailed study of peat $^{14}C$ dating (Misra et al., 2024), our previous studies call for cautions on $^{14}C$ chronology which depends on a few $^{14}C$ dates on TOC in lake sediments. Since accurate chronology of a lake record is an essential foundation for high-resolution paleoenvironmental reconstruction, more well-dated lake records are certainly needed over the Russian territory.

In Russia, many lake records are based on biological proxies such as pollen, diatom, chironomid and Cladocera (e.g. Frolova and Nigmatullin, 2019; Frolova et al., 2022; Nigmatullin et al., 2022; Nigamatzyanova et al., 2024; Nazarova et al., 2025), while a much lower number of lake records use elemental analyses determined by either X-ray Fluorescence (XRF), or Inductively Coupled Plasma (ICP) and ICP-Optical Emission Spectrometry (OES) measurements on Aqua Regia + microwave digested solution (Bertrand et al., 2024). The elemental contents through the above analyses contain large contributions from detrital materials which do not reflect lake chemistry (Blyakharchuk et al., 2020; Li et al., 2022; Misra et al., 2025). Instead, weak acid (<1N HCl) leachable elements which are dissolved from carbonates, authigenic minerals and adsorption phases can provide information of lake chemistry (Li et al., 2000, 2004; Misra et al., 2025). Therefore, the weak acid-leachable elements should be used for deciphering lake chemistry change even though the analytical procedure requires more time and work.

Pollen records also show some complications as many arboreal taxa pollen (AP) grains are able to be transported for long distances (hundreds of kilometers), and thus, reflect regional vegetation. In contrast, non-arboreal pollen (NAP) grains are originated mainly from local vegetation and better reflect local vegetation cover (El-Moslimany, 1990; Broström et al., 2008; Gaillard et al., 2008; Lu et al., 2022). Studies of the relationship between pollen assemblages and climatic conditions in dry regions demonstrate that AP content has a positive relationship with mean annual precipitation (MAP), whereas herb pollen ratio *Artemisia*/Chenopodiaceae (A/C) is positively linked to MAP, but *Artemisia*/Cyperaceae (A/Cy) ratio has a positive relationship with mean annual temperature (MAT) (Herzschuh, 2007; Qin et al., 2015; Li et al., 2016a; Zhang and Feng, 2018; Cui et al., 2019; Lü et al., 2020; Welc et al., 2021; van Vugt et al., 2022; Shichi et al., 2023; Ma et al., 2024). However, changes in wind systems could also affect the pollen source, consequently influence the AP/NAP ratio (e.g., Lü et al., 2020). Both temperature and precipitation can influence *Artemisia* and Cyperaceae abundances. So, does an increased *Artemisia*/Cyperaceae (A/Cy) ratio reflect a MAT or MAP increase? Similarly, considering wind direction change, does an AP/NAP increase (or decrease) represent higher MAP or lower MAT shift? Hence, although pollen record is an important tool in reconstruction of paleoenvironmental conditions, multiple influencing factors such as temperature, precipitation, wind direction/speed and sedimentary process may complicate the interpretation of climate and environmental conditions if only depending on pollen records. Therefore, comparisons among instrumental records, geochemical records and pollen records from the same area especially from the same lake record can help interpreting pollen assemblages.

While temperature is mainly controlled by variations in solar energy and its influx to the earth and tends to vary in the same direction over large regions, changes in precipitation towards wetter/drier conditions can vary spatially within the same region depending on geographic settings and atmospheric-oceanic circulations (Chu et al., 2012; Neukom et al., 2019; Tang et al., 2025). RWP, DACP, MCA, LIA, and CWP are significant climate phases within the past 2000 years (Mann et al., 2009; Lamb, 2011; Helama et al., 2017; Shi et al., 2021). The RWP, MCA and CWP were warm periods, while the DACP and LIA were cold periods. However, the moisture conditions in the study area did not agree with warm/wet and cold/dry patterns (Chen et al., 2015; Blyakharchuk et al., 2017). Thus, what was the precipitation pattern and what was the forcing factor of moisture conditions in the study area during those warm and cold periods?

This paper presents multi-proxy records from a well-dated 64-cm long core from Zolotoe Lake located in the West Siberian Plain (Russia). The dating methods involve $^{210}Pb$, $^{137}Cs$ and AMS $^{14}C$. The proxy records include TOC, TN, C/N, 0.5N HCl leachable (AL) and Aqua Regia dissolution (AR) elemental concentrations measured by ICP-OES, pollen assemblages, and mineral compositions measured by X-ray Diffraction (XRD) and Scanning Electron Microscope (SEM). AMS $^{14}C$ ages on acid (A-) and acid-base-acid (ABA-) treated sedimentary TOC are used not only to provide a reliable chronology of the core over the past 1800 years, but also to uncover the old carbon influence (OCI) on some $^{14}C$ ages. Comparisons of AL and AR elements allow us to understand their geochemical meanings and applications in paleoclimate and paleoenvironmental reconstructions using lake sediments. The pollen record is compared with changes in the lake chemistry under different climatic conditions as well as with the instrumental weather records to illustrate the relationships of AP/NAP and A/Cy ratios to climatic conditions in terms of MAT and MAP. Finally, this study describes climatic conditions, vegetation coverage, and human activity during the RWP, DACP, MCA, LIA and CWP.

## 2. Study area

The study area is located in the southern part of West Siberia, Russia, spanning approximately 600 km from east to west and about 400 km from north to south. This region lies between two distinct terrain types:

the West Siberian Plain and the Altai-Sayan foothills of the Salair and Altai Mountains. The mountainous areas are situated to the east and southeast of the plains. The western and central regions feature the Ob Plateau, with an average elevation of 250–260 m above sea level (a.s.l.), the Biysk-Chumysh Highlands, and the Kulunda Plain, which has an average elevation of approximately 400 m a.s.l. Altai Krai encompasses nearly all of Russia's natural landscapes, including steppe, forest steppe, boreal forest, and mountainous regions (Fig. 1). The study area is

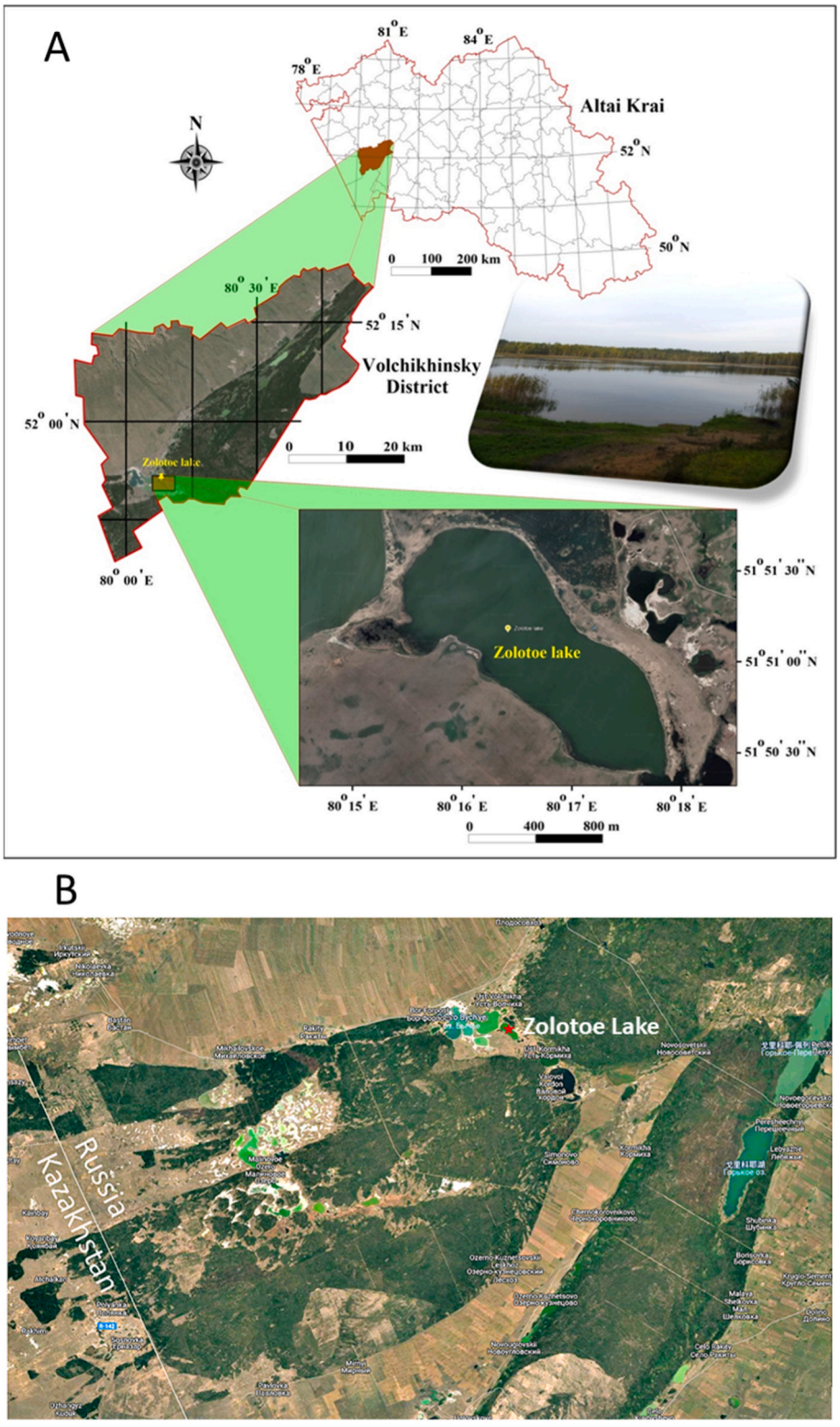


**Fig. 1.** Location map of the study area and Zolotoe Lake. A. A sketch map of Altai Krai is on the top. The dark red area in the sketch map denotes the Volchikhinsky district which contains Zolotoe Lake in the south. A photo of Zolotoe Lake is shown on the middle right. The sediment core site is located in the center of the lake. B. A satellite photo of the study area downloaded from Google Map shows Zolotoe Lake (red star) and its surrounding area. Farmland, playas and lakes can be seen. The dark green area reflects the Kasmalinsky and Barnaul ribbon forests in low hills.

centered in the Kulunda Plain which is characterized by its flat, low-lying topography formed by Quaternary sediments and glacial deposits. Due to ancient glacial events, erosion and meltwater deposition, this area contains many lakes including the Volchikhinsky lake system. Since the 1930s CE, large areas were converted to farmlands in the flat zones (Andreenkov, 2021). The Volchikhinsky lake system includes several dozen reservoirs (lakes) located in ancient drainage depressions and surrounded by ribbon pine forests at the confluence of the Kasmalinsky and Barnaul ribbon forests which are a narrow belt of low hills lining from southwest to northeast (Fig. 1B). The lakes of recreational significance include Bychye, Zolotoe, Domashnee, Valovoye, Maralye, Beloe, and Gorkoye. The area has also many playas, which may be remnants of former lakes. Under wet climate conditions, those playas and lakes might be connected to each other.

Zolotoe Lake (51°51′28.74″N, 80°15′59.16″E) is situated in the ribbon forest of the Kulunda Plain within the West Siberian Lowland of Russia (Fig. 1). This shallow lake covers an area of 3.8 $km^2$ at an elevation of 207 m a.s.l. (Bykov et al., 2023). The region is characterized by a continental climate with long, cold and relatively dry winters from November to March and temperatures ranging from −40 to +1 °C. The summers are short and relatively warm with temperatures between +16 and + 33 °C from June to August. Spring (April to May) is characterized by temperatures ranging from +3 to +21 °C, while autumn spans from September to October, with temperatures between −5 and +23 °C. The winter season, marked by ice cover on Volchikhinsky District lakes, typically lasts from late October to late March (Bykov et al., 2023). Barnaul Meteorological Station is the nearest weather station and has the longest temperature record (since 1838 CE) and precipitation record (since 1966 CE). In this study, the weather data are ended at 2016 CE. Based on the air temperature from 1838 to 2016 CE and precipitation from 1966 to 2016 CE, the MAT and MAP are 1.3°C and 426 mm/yr, respectively. Fig. S1 shows the mean monthly air temperature and precipitation.

The vegetation surrounding the lake is diverse. *Pinus sylvestris*, *Populus*, *Betula alba*, *Salix*, *Crataegus*, *Rosa*, and *Viburnum* grow in the direct vicinity of the lake (Dirin et al., 2017). The northern coast is occupied by a pine forest, while the coastal areas are covered with halophytic and hydrophytic vegetation. The main plant communities in the study area are coastal zone habitats (such as reed-cattail formations), fescue steppes, shrubby grass-forb meadow steppes, halophytic salt marsh vegetation, shrubland, sedge-aspen forests, and dry-steppe sedge pine forests (Skaldina and Slizh, 2018). The lake is actively used for recreational purposes (Dirin et al., 2017).

## 3. Methods

### 3.1. Field work and subsampling

A 64-cm long core (22-Al-03A) was collected using a Russian cylindrical core sampler with a vacuum seal "Taifun" (diameter 82 mm, length 120 cm) from the center of Zolotoe Lake in 2022 by a team from Kazan Federal University (KFU) and V.S. Sobolev Institute of Geology and Mineralogy of the Siberian Branch of the Russian Academy of Sciences, Russia. In the field, the core was split into three slides for observation, description and subsampling. Based on the texture and color, the core can be classified into four sections: 64-52 cm, grey clay; 52-37 cm, dark grey mud; 37-21 cm, coarse brown mud; and 21-0 cm, soapy fine brown mud (Fig. 2). The core was subsampled in the field at 2 cm intervals for high-resolution paleoclimate studies. The subsamples were sealed in plastic bags and stored at 4 °C in a refrigerator for further studies. At KFU, the samples were freeze-dried and divided into aliquots for AMS $^{14}C$ dating, gamma spectrometry, and both geochemical and biological analyses. According to the geochemical proxies, texture and color of the core, six zones were identified with the sedimentation rates

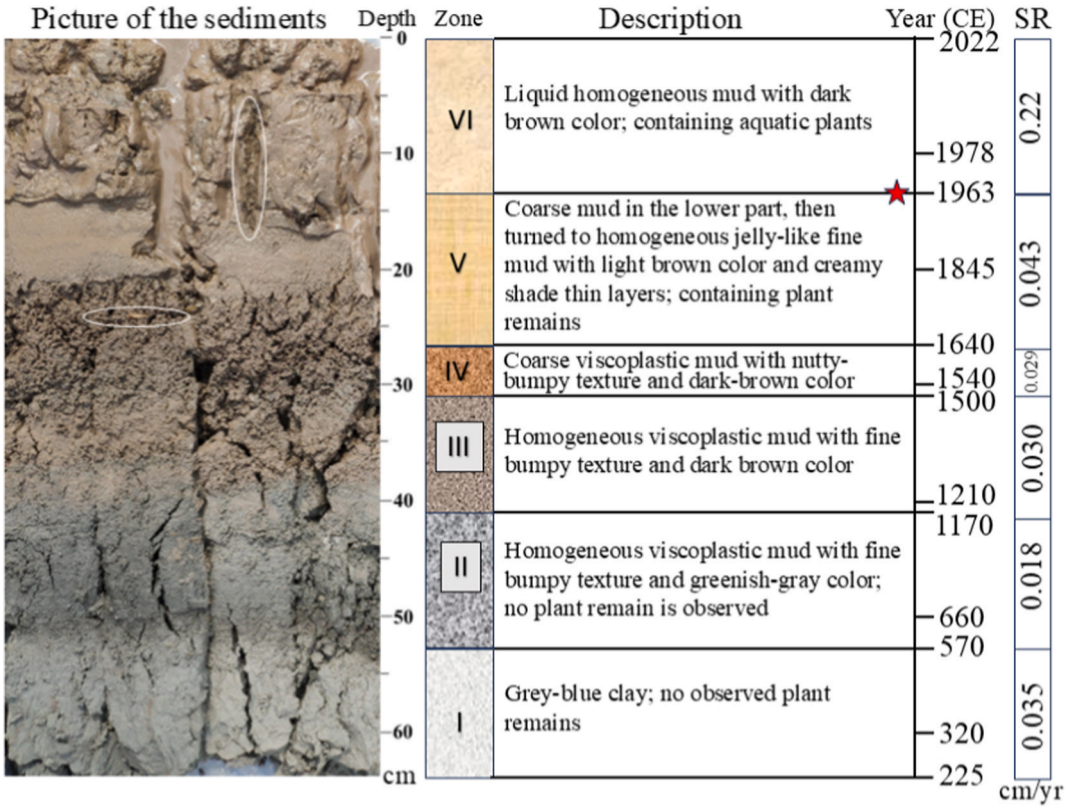


**Fig. 2.** Photograph and description of the core 22-Al-03A. The picture was taken in the field after the core was cut in three pieces. The white oval circles in the picture indicate the plant remains in the core. Zones are determined by features of the sediments, geochemistry and pollen assemblages. The red star denotes the depth of the $^{137}Cs$ peak which reflects the deposition at 1963/64 CE. Ages and sedimentation rates are determined by $^{210}Pb$, $^{137}Cs$ and AMS $^{14}C$ dating.

listed in Fig. 2.

### 3.2. Gamma dating ($^{210}$Pb and $^{137}$Cs)

The activities of radionuclides $^{210}$Pb, $^{238}$U, $^{226}$Ra, $^{214}$Pb, $^{232}$Th, $^{137}$Cs and $^{40}$K in the sediments were measured by using an ORTEC low-background semiconductor gamma spectrometer at the NTUAMS laboratory, Department of Geoscience, National Taiwan University (NTU), Taiwan. The freeze-dried samples, weighing between 1.13 g and 5.26 g, were ground to a particle size of less than 63 μm and placed in a 6-cm diameter container for gamma counting following Li et al. (2019, 2022) and Misra et al. (2025). The supported $^{210}$Pb activity was determined using the activity of $^{226}$Ra, as measured via $^{214}$Pb activity at 353 keV. Excess $^{210}$Pb activity was calculated by subtracting the supported $^{210}$Pb activity from the total $^{210}$Pb activity. The precision of gamma counting was within ±5% at the 95% confidence level. The $^{210}$Pb chronology was established using the constant flux model (Appleby and Oldfield, 1992). In the $^{137}$Cs profile, the peak depth reflects the maximum fallout from the global atmospheric thermonuclear weapon tests in the year of 1963 CE (Hardy, 1971; Ritchie et al., 1973).

### 3.3. AMS $^{14}$C dating

AMS $^{14}$C dating was performed at the NTUAMS Lab using a 1.0 MV Tandetron Model 4110 BO AMS following the description of Li et al. (2022). The best materials in lake sediments for $^{14}$C dating are terrestrial plant remains deposited in the sediments. However, the studied core lacks such plant macrofossils. As shown in Fig. 2, plant remains were not found below 20 cm core depth. Two aquatic plant remains appeared on the upper 20 cm (Fig. 2), but the upper one was a 10-cm long aquatic grass with no specific depth and the lower one was ignored during subsampling. Thus, the $^{14}$C dating of this study was carried out on the TOC in the sediments. In order to eliminate the influence of inorganic carbon (carbonates) and mobilized organic acid (such as humic and fulvic acids), sediment samples need to go through pre-treatments: either acid (A) or acid-base-acid (ABA) methods. Although $^{14}$C dating on lake sediments has commonly used ABA pretreatment to remove carbonates and organic acids, our previous studies have shown that the $^{14}$C ages of the same TOC sample may have significant differences for A- and ABA-treated fractions (Blyakharchuk et al., 2020; Misra et al., 2024, 2025). In some cases, the $^{14}$C age of ABA-treated sample is significantly older than that of the A-treated sample from the same sedimentary TOC, due to uptake of dissolved $CO_2$ from the lake water during the photosynthesis of aquatic plants. Thus, we carried out AMS $^{14}$C dating on both A- and ABA-treated TOC from the same samples in 18 horizons. A total of 38 AMS $^{14}$C dates were obtained for 20 horizons of the core, divided into two treatment groups following the instructions of Misra et al. (2024, 2025). The first group was conducted in May 2024, involving 18 0.5N HCl (A-) treated samples. The second group was carried out in July 2024, involving 20 Acid-Base-Acid (ABA-) samples. The ABA treatment was following the procedure outlined by Brock et al. (2010). The extraction of $CO_2$ and graphitization of all treated samples were performed by a homemade semiautomatic graphitization device (Shen et al., 2024). The measured $^{14}C/^{12}C$ and $^{13}C/^{12}C$ ratios by the AMS for standards (OXII), background (BKG) and samples were used for $^{14}$C age calculation including $\delta^{13}$C fractionation (Li et al., 2022). The $^{14}$C ages were calibrated with IntCal20 calibration curve (Reimer et al., 2020). All calibrated $^{14}$C ages in the study are expressed as cal yr BP (i.e. calibrated years before the present, fixed at 1950 CE by convention).

### 3.4. Elemental analysis (EA) of organic matter

About 300 mg of original sample was weighed for acid leaching, AMS $^{14}$C dating and organic matter analyses as all three analyses need to separate organic and inorganic carbons (see Section 3.5). Approximately 20 mg of each acid-leached sample was accurately weighed, placed into a small tin cup, and loaded into an auto-sampler. Total organic carbon (TOC) and nitrogen (TN) were quantified by using a Thermo Scientific Flash 2000 Elemental Analyzer (EA) at the NTUAMS Lab. The sample was combusted in a quartz tube with $O_2$ at 950 °C. The resulting gases then reacted with tungsten oxide, which provided additional oxygen as a catalyst to ensure complete combustion and prevent the formation of non-volatile sulfates. The gases were subsequently reduced by reacting with electrolytic copper at 600°C in the second quartz tube. The elemental analyzer was calibrated using a 2,5-Bis (5-tert-butyl-2-benzoxazol-2-yl) thiophene (BBOT) standard, which was measured after every five samples to ensure precision in the results.

### 3.5. Elemental concentrations measured by ICP-OES

A total of 32 core samples for both 0.5N HCl leaching fraction (AL) and Aqua Regia dissolution fraction (AR) were analyzed. For the AL sample analysis, ~300 mg of each original samples were weighted and placed into a 50-ml centrifuge tube and leached with 15 ml of 0.5N HCl solution. This procedure effectively removes inorganic carbon (primarily carbonate impurities) and adsorbed oxides from the particle surfaces, while preserving the organic components and detrital phases within the sediments. The AL elements are considered to represent the active fraction, reflecting the chemical conditions and productivity in the water column (Li et al., 2000, 2004, 2022). Following centrifugation, the acid solution was adjusted to a final volume of 50 ml using a volumetric flask. The resulting solution was then analyzed using a PerkinElmer (PE) Optima 8000DV Inductively Coupled Plasma Optical Emission Spectroscopy (ICP-OES) at the NTUAMS Laboratory. The solid residue was oven dried and weighed for calculation of the acid leach weight loss (ALWL% = $(W_s - W_r) \times 100/W_s$, $W_s$ and $W_r$ are weight of sample and residue, respectively).

For the AR sample analysis, approximately 100 mg of original samples from each depth were precisely weighed and subsequently digested with Aqua Regia, a mixture of concentrated acids in a 1:3 ratio (1 ml of $HNO_3$ + 3 ml of HCl). The dissolution process was conducted in a 100 ml glass beaker which was heated on a hot plate under 90°C overnight. The residue in the beaker was dissolved with 15 ml 4N $HNO_3$ and transferred into a 50-ml centrifuge tube. After centrifuging, the supernatant was transferred into a 50-ml volumetric flask. The solid in the centrifuge tube was then washed with de-ionized water (DIW) and centrifuged again. The supernatant was combined into the volumetric flask. This washing procedure was repeated one more time. Finally, DIW was added to the combined solution up to the 50-ml mark of the volumetric flask. The solid residue was dried in oven and weighed for calculation of weight loss by the dissolution (Aqua Regia digestion weight loss, ADWL %). The solution was then analyzed for selected elements, similar to those measured for the AL elements, using ICP-OES at the NTUAMS Lab.

Twenty-one elements (Al, Ba, Ca, Cr, Cu, Fe, Ga, K, Mg, Mn, Mo, Na, Ni, P, Pb, Rb, Si, Sr, Ti, U, Zn) were analyzed by the ICP-OES at the NTUAMS Lab. Elemental concentrations measured by the ICP-OES were determined by using standard curves derived from various concentrations of standard solutions. The correlation coefficient ($R^2$) of the intensity-concentration relationship for each element was typically greater than 0.995. The measurement uncertainty was approximately 0.2% at a concentration level of 1 mg/L (ppm).

### 3.6. Pollen analysis

Pollen samples, each consisting of 0.8-1.2 g of the dry sediment, were treated for pollen analysis according to Fægri and Iversen (1989). One *Lycopodium clavatum* spore tablet was added to each sample to calculate pollen and spore concentration (Stockmarr, 1971). Microscopic analysis was carried out under a magnification of × 400. A minimum of 350 pollen grains per sample were counted.

The total pollen sum used for determination of relative frequencies includes terrestrial pollen. Stratigraphic zonation of the pollen data was

performed using CONISS (Grimm, 1987). Tilia/TiliaGraph software version 3.0.1 (Grimm, 2004) was used for the calculation of percentages and for drawing the pollen diagram. As the focus of this study is on the major features of the vegetation changes, not all identified species were plotted in the pollen diagram.

### 3.7. Mineral analysis by X-ray diffraction (XRD)

A total of nine samples from the core were selected for investigating mineralogical composition. The selection of the XRD samples is mainly based on changes in the lithological, color and density of the core shown in Fig. 2. The analysis was conducted by using X-ray diffraction (XRD) with a D2 instrument at the Institute of Mineral Resources Engineering, National Taipei University of Technology (NTUT). The instrument was equipped with a scintillation NaI photomultiplier and a preamplifier. Approximately 50 mg of each sample was finely ground to a particle size smaller than 270 mesh. A suitable amount of the powdered sample was placed in a small circle at the center of the holder, and its surface was leveled to eliminate any excess powder. The operating conditions were as follows: rated outputs of 3000 V and 4 kW; a Cu-target tube voltage of 50 kV; a Ni filter current of 40 mA; two theta angles ranging from 10° to 70°; and a scan speed of 2.00°/min. The XRD system was connected to a computer system for data diffraction and measurement. Data analysis was performed using Jade software.

### 3.8. Scanning Electron Microscope (SEM) measurements

The same 9 samples as for XRD analysis were also measured by a JSM-6510 Scanning Electron Microscope (SEM) at the SEM Lab of NTUT. The facility provides SEM imaging and chemical composition analysis determined by energy-dispersive X-ray spectroscopy (EDX). The SEM was operated under the following conditions: acceleration voltage of 15 kV, current of 10 nA, acquisition time of 60 s, and spot size of 50 μm. The chemical composition of the sediments was analyzed by examining EDX peaks. The sediment samples were coated with gold using a JFC-1600 Auto Fine Coater. In addition, SEM measurements were also performed by Sobolev Institute of Geology and Mineralogy, SBRAS, which provided some mineral compositions of the sediments.

## 4. Results

### 4.1. $^{210}$Pb and $^{137}$Cs dating results

Table S1 in the supplement materials lists the results of measured radionuclides by gamma spectrometry. The measured $^{210}$Pb activity is significantly higher than that of $^{226}$Ra (i.e., supported $^{210}$Pb) throughout the core, indicating that $^{226}$Ra in the sediments is depleted (i.e., $^{210}$Pb and $^{226}$Ra are not in secular equilibrium) mainly due to $^{222}$Rn degassing. This phenomenon is quite common in lake sediments. Figure. 3A shows that the total $^{210}$Pb activity above 19 cm depth follows an exponential decay trend. Using the excess $^{210}$Pb profile (total $^{210}$Pb minus supported $^{210}$Pb activity), an exponential fitting yields the slope of −0.146 ($R^2$ = 0.84) which results in an average sedimentation rate of 0.213 cm/yr (Fig. 3A) (Appleby and Oldfield, 1992). This constant initial excess $^{210}$Pb implies the following conditions: (1) a constant deposition rate of fallout $^{210}$Pb (both constant initial excess $^{210}$Pb activity and linear sedimentation rate); (2) immobility of $^{210}$Pb within the sediment column (Appleby, 2000; Saulnier-Talbot et al., 2009). The fitting result strongly depends on the ending point of excess $^{210}$Pb activity (the lowest point in the profile) and fitting coefficient ($R^2$). The higher the $R^2$, the smaller the uncertainty will be. With $R^2$ = 0.84, the reliability of the $^{210}$Pb dating should be reinforced by additional proxies, such as $^{137}$Cs.

$^{137}$Cs is an artificial and anthropogenic radionuclide generated by nuclear bomb tests and nuclear power plants, with a half-life of 30.2 years (Hardy, 1971; Ritchie et al., 1973; Michel et al., 2002). Fig. 3B shows that the $^{137}$Cs peak occurred at 13 cm depth (sample 12-14 cm) corresponding to the year of 1963 CE (Hardy, 1971; Ritchie et al., 1973). Using the two known age depths: the coring year of 2022 CE at 0 cm depth and 1963 CE at 13 cm depth, a linear sedimentation rate for the upper 13 cm is estimated to be 0.22 cm/yr (Fig. 3B). This $^{137}$Cs-estimated linear sedimentation rate (0.22 cm/yr) agrees well with the $^{210}$Pb-estimated sedimentation rate (0.213 cm/yr). However, the sedimentation rate estimated by $^{137}$Cs is more certain than that of $^{210}$Pb-estimated due to the clear and outstanding $^{137}$Cs peak. Thus, we can use 0.22 cm/yr to determine the ages for the sediments in the upper 13 cm. The ages for the upper 13 cm are listed in the last column of Table S1.

### 4.2. AMS $^{14}$C dating results

Table 1 lists 38 AMS $^{14}$C dates for the sedimentary TOC from 20

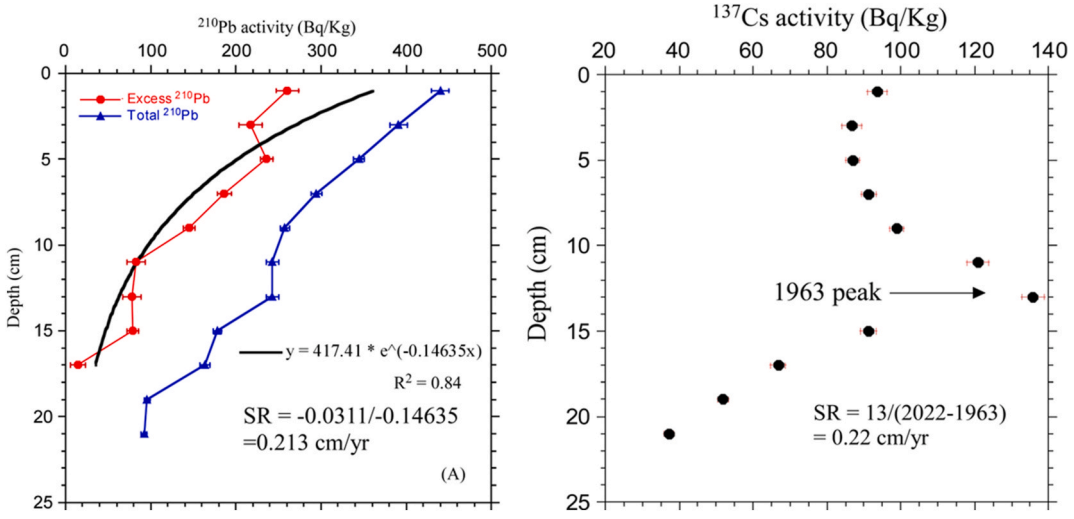


**Fig. 3.** Gamma dating results. (A) $^{210}$Pb profile. The excess $^{210}$Pb is the total $^{210}$Pb activity after subtracting the $^{226}$Ra activity. An exponential fitting of the excess $^{210}$Pb yields a linear sedimentation rate (SR) of 0.213 cm/yr (B) $^{137}$Cs profile. The sharp $^{137}$Cs peak at 12-14 cm depth (middle depth is 13 cm) points the age of 1963 CE. A linear sedimentation rate of 0.22 cm/yr can be obtained for the upper 13 cm sediments.

**Table 1**
AMS $^{14}$C results of samples from 22-Al-03A core. All Lab codes have a EAAMS prefix. All sample IDs have a 22-Al-03A prefix. All sediment samples have been treated with either acid (A) or acid-base-acid (ABA) process. pMC stands for percent of modern $^{14}$C. The last column lists the age used for Bacon model marked with Y.

| Lab Code | Sample ID | Depth (cm) | pMC (%) | Conventional $^{14}$C Age (yr BP) | Calibrated $^{14}$C Age (Cal yr BP) | Bacon model |
|---|---|---|---|---|---|---|
| 401 | _0-2 cm A | 1 | 105.50 ± 0.66 | −430 ± 50 | modern | Y |
| 497 | _0-2 ABA | 1 | 105.76 ± 0.77 | −450 ± 58 | modern | Y |
| 402 | _2-4 cm A | 3 | 108.05 ± 0.65 | −622 ± 48 | modern | Y |
| 498 | _2-4 ABA | 3 | 106.42 ± 0.85 | −500 ± 64 | modern | N |
| 403 | _4-6 cm A | 5 | 106.81 ± 0.90 | −529 ± 68 | modern | Y |
| 499 | _4-6 ABA | 5 | 108.89 ± 0.69 | −684 ± 51 | modern | N |
| 404 | _6-8 cm A | 7 | 108.51 ± 0.79 | −656 ± 58 | modern | Y |
| 500 | _6-8 ABA | 7 | 102.55 ± 0.80 | −202 ± 63 | modern | N |
| 405 | _8-10 cm A | 9 | 109.32 ± 0.61 | −716 ± 45 | modern | Y |
| 501 | _8-10 ABA | 9 | 107.50 ± 0.92 | −581 ± 68 | modern | Y |
| −406 | _10-12 cm A | 11 | 109.40 ± 0.79 | −722 ± 58 | modern | N |
| 502 | _10-12 ABA | 11 | 108.74 ± 0.56 | −673 ± 41 | modern | Y |
| 383 | _12-14 cm A | 13 | 107.87 ± 0.75 | −609 ± 56 | modern | N |
| 503 | _12-14 ABA | 13 | 109.97 ± 0.68 | −763 ± 49 | modern | Y |
| 407 | _14-16 cm A | 15 | 101.01 ± 0.84 | −81 ± 67 | modern | Y |
| 504 | _14-16 ABA | 15 | 107.37 ± 0.68 | −571 ± 51 | modern | N |
| 408 | _16-18 cm A | 17 | 101.22 ± 0.63 | −98 ± 50 | modern | Y |
| 505 | _16-18 ABA | 17 | 98.41 ± 0.62 | 128 ± 51 | 80 ± 75 | N |
| 409 | _18-20 cm A | 19 | 98.98 ± 0.75 | 82 ± 61 | modern | Y |
| 506 | _18-20 ABA | 19 | 95.37 ± 0.72 | 381 ± 61 | 415 ± 105 | N |
| 384 | _22-24 cm A | 23 | 98.03 ± 0.79 | 160 ± 65 | 145 ± 145 | Y |
| 507 | _22-24 ABA | 23 | 96.77 ± 0.54 | 264 ± 45 | 365 ± 100 | N |
| 508 | _26-28 ABA | 27 | 94.93 ± 0.56 | 418 ± 47 | 480 ± 55 | N |
| 385 | _30-32 cm A | 31 | 95.58 ± 0.67 | 363 ± 56 | 410 ± 100 | Y |
| 509 | _30-32 ABA | 31 | 93.00 ± 0.69 | 583 ± 60 | 590 ± 70 | N |
| 410 | _34-36 cm A | 35 | 93.41 ± 0.81 | 548 ± 70 | 580 ± 85 | Y |
| 510 | _34-36 ABA | 35 | 100.30 ± 0.55 | −24 ± 44 | modern | |
| 386 | _40-42 cm A | 41 | 89.71 ± 0.69 | 872 ± 62 | 765 ± 80 | Y |
| 511 | _40-42 ABA | 41 | 90.78 ± 0.73 | 777 ± 65 | 715 ± 85 | Y |
| 411 | _44-46 cm A | 45 | 87.96 ± 0.56 | 1031 ± 51 | 980 ± 80 | Y |
| 512 | _44-46 ABA | 45 | 86.93 ± 0.50 | 1125 ± 46 | 1045 ± 90 | Y |
| 387 | _50-52 cm A | 51 | 83.40 ± 0.69 | 1458 ± 66 | 1455 ± 25 | Y |
| 513 | _50-52 ABA | 51 | 80.49 ± 0.81 | 1743 ± 81 | 1670 ± 160 | N |
| 412 | _54-56 cm A | 55 | 81.49 ± 0.54 | 1645 ± 53 | 1515 ± 115 | Y |
| 514 | _54-56 ABA | 55 | 81.71 ± 0.71 | 1622 ± 70 | 1495 ± 135 | Y |
| 515 | _60-62 ABA | 61 | 79.56 ± 0.68 | 1837 ± 69 | 1735 ± 165 | N |
| 388 | _62-64 cm A | 63 | 80.01 ± 0.58 | 1792 ± 58 | 1690 ± 135 | Y |
| 516 | _62-64 ABA | 63 | 79.44 ± 0.71 | 1849 ± 71 | 1760 ± 175 | Y |

horizons of 22-Al-03A core. Amongst the 38 $^{14}$C dates, the age of 22-Al-03A 34-36 cm ABA (EAAMS-510) does not conform (perhaps the analysis failed due to leakage to the atmosphere), and was not retained in the age model developed for this study (Table 1). Fig. 4A plots the rest 37 $^{14}$C dates. Three observations can be made. (1) The values of pMC (percent modern carbon) above 18 cm depth are >100%, which means that the samples contain nuclear bomb $^{14}$C and younger than 1950 CE (Hua et al., 2022). (2) The highest pMC is around 13 cm depth (sample

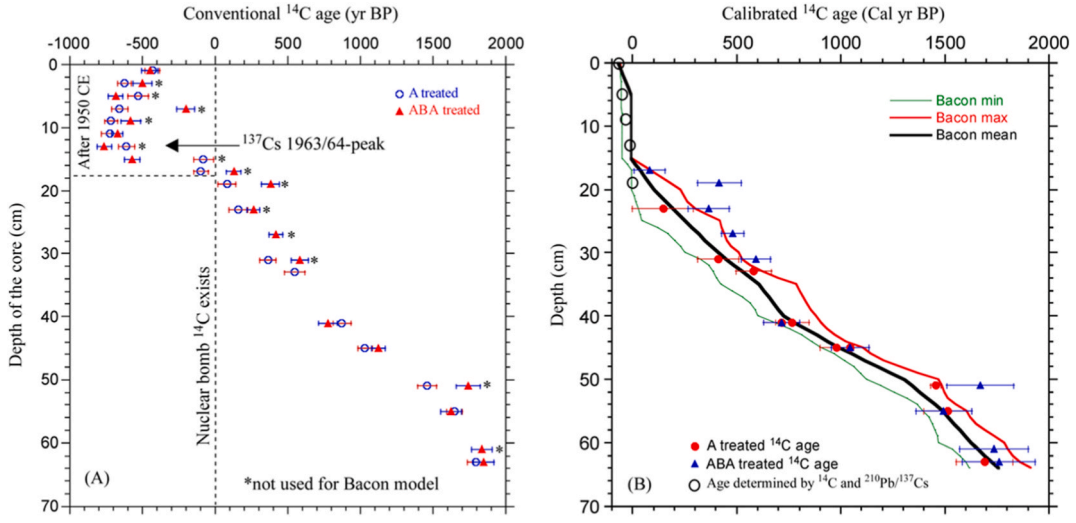


**Fig. 4.** AMS $^{14}$C dating results and chronology of the core 22-Al-03A. (A) Measured (uncalibrated) $^{14}$C ages of the sedimentary TOC. Most of the samples contain paired ages of 0.5 N HCl acid (A-) treated and acid-base-acid (ABA-) treated fractions. The * symbol denotes the ages which were affected by the old carbon influence, so they were not used for chronology construction. (B) Bacon age-depth model of the core 22-Al-03A. The modelled chronology above 19 cm depth is incorrect based on $^{14}$C ages. Instead, the chronology for the upper 19 cm part is determined by the sedimentation rates from $^{210}$Pb and $^{137}$Cs dating.

12-14 cm), agreeing with the $^{137}$Cs peak very well. This result confirms that the upper 13 cm have a mean sedimentation rate of 0.22 cm/yr and that the 14-16 cm and 16-18 cm layers must have been deposited after 1950 CE. Assuming an age of 1950 CE is for the 18-cm depth, the sedimentation rate between 14 cm and 18 cm depths should be 0.3 cm/yr, indicating that a strong increase in sedimentation rate occurred during this period. (3) Below 18 cm depth, the ABA-treated ages are either the same as (within the uncertainty) or older than their paired A-treated ages, indicating old carbon influence (OCI) on the ABA-treated fraction $^{14}$C age (Misra et al., 2024). The lake chemistry varied with time under climatic changes and anthropogenic influences. In periods when lake alkalinity and salinity are high, dissolved $CO_2$ increases in the lake water, and the reservoir effect of the lake might be increased. Organic matters such as algae and submerged aquatic plants may use the dissolved $CO_2$ to form humin through photosynthesis (Cook et al., 1998; Chen et al., 2021; Misra et al., 2024, 2025). Under such a circumstance, the A-treated sample is considered more reliable than the ABA-treated sample because carbonate and fulvic acid (regarded as secondary mobile products after sediment deposition) can be removed by 0.5N HCl treatment, leaving humic acid and humin for dating which are thought to more accurately reflect the time of the organic matter formation (Cook et al., 1998; Ascough, 2014; Misra et al., 2024, 2025). In contrast, ABA treatment will remove carbonate, fulvic acid and humic acid, and leave humin alone for dating (Brock et al., 2010), so that its $^{14}$C age demonstrates more reservoir effect (Misra et al., 2024, 2025). The ABA-treated $^{14}$C ages at 12-14 cm and 14-16 cm depths were younger than their paired A-treated $^{14}$C ages (Fig. 4A and Table 1) which was opposite to the OCI mentioned above. In fact, this phenomenon exists in the peat study of Misra et al. (2024). Near the nuclear bomb $^{14}$C peak time, the $^{14}C/^{12}C$ ratio of dissolved $CO_2$ in lake water may be higher than that of surface runoff, depending on the $^{14}$C activity of the decomposed organic carbon. For instance, the pore water $CH_4$ in peatlands was enriched in $^{14}$C relative to the peats at the same depth horizon during the post-bomb period (Aravena et al., 1993; Charman et al., 1994; Chanton et al., 1995). Compared to the $^{14}$C age of *Carex* leaf from the same ABA-treated samples, younger $^{14}$C ages in the *Carex* roots appeared in the post-bomb interval, but older $^{14}$C ages in the *Carex* roots existed in the pre-bomb interval, indicating uptake of dissolved $CO_2$ from peat water (Misra et al., 2024). Zolotoe Lake is a shallow and organic carbon rich lake, and contains abundant aquatic plants.

In summary, the AMS $^{14}$C dating results show: (1) the nuclear bomb $^{14}$C signal is recorded in the sedimentary TOC above 19 cm (sample 18-20 cm) depth with the 1963 CE peak at 13 cm (sample 12-14 cm) depth. The calibrated $^{14}$C age of sample 18-20 cm is close to 1950 CE; (2) Reservoir effect can cause OCI in TOC due to uptake of dissolved $CO_2$ by aquatic plants and algae when the lake had high salinity and alkalinity. ABA-treated $^{14}$C age is generally older than its paired A-treated $^{14}$C age due to removal of humic acid except close to the nuclear bomb $^{14}$C peak. Most of the A-treated and ABA-treated pairs have the same $^{14}$C age within uncertainty, reflecting no OCI on those ages. In total, 14 $^{14}$C ages were retained to develop the age model using the Bacon programme (Table 1).

### 4.3. Chronology of the core

With the gamma dating and AMS $^{14}$C dating results, we are able to establish a robust chronology of the 22-Al-03A core. According to $^{210}$Pb and $^{137}$Cs dating results, a sedimentation rate of 0.22 cm/yr has been obtained. Based on this rate, the calculated ages of 17 cm (sample 16-18 cm) and 19 cm depth (sample 18-20 cm) should be 1949 CE and 1906 CE, respectively, which means that these two layers should be deposited before 1950 CE with no nuclear bomb $^{14}$C signal. However, our AMS $^{14}$C measurements do not agree with this estimation (Table 1). Previous studies have found that both $^{210}$Pb and $^{137}$Cs in lake sediments may experience a post-depositional mobilization especially in acidic water (Rowan et al., 1992; Le Roux and Marshall, 2011; Baskaran et al., 2017; Li et al., 2019; Misra et al., 2024). But, as described in Section 4.2, the peak of $^{14}$C activity appeared in 12-14 cm depth, strongly agreeing with the $^{137}$Cs peak. Therefore, $^{137}$Cs peak downward shift did not occur in this core. Hence, the 0.22 cm/yr sedimentation rate can only apply to the layers above 12-14 cm depth (i.e., after 1963 CE). Nevertheless, the chronology of the sediments below the $^{137}$Cs peak must be determined by $^{14}$C dating. As mentioned in Section 4.2, the calibrated $^{14}$C age of A-treated sample 18-20 cm is close to 1950 CE (Table 1). Using 1963 CE at 13 cm and 1950 CE at 19 cm depths, a sedimentation rate of 0.856 cm/yr is obtained, which is much higher than the average rate after 1963 CE. This high sedimentation rate is the result of human activity due to the development of farmland around the lake (Andreenkov, 2021). But, the development of farmland in this area started in the 1930s according to the historical documents, which suggests that the calculated sedimentation rate of 0.856 cm/yr may not be accurate. Therefore, a more practical approach is to use the available $^{14}$C dates for establishing a chronology and combine them with the gamma dating results. To this aim, the Bacon age-modelling software (Blaauw and Christen, 2011) was used to develop an age-depth (Table 1, Fig. 4B). However, a couple of problems are apparent in the modelled results: (1) the modelled ages not only disagree with the $^{137}$Cs dating results but also remain unchanged between the 5 cm and 15 cm. depths (thick black line in Fig. 4B); (2) the modelled ages for the depths between 13 cm and 20 cm are older than excepted. For example, the Bacon mean ages for depths of 16-18 cm and 18-20 cm were 35 cal yr BP (1915 CE) and 79 cal yr BP (1871 CE), respectively. However, both layers contain nuclear bomb $^{14}$C signal (after 1950 CE). To solve the first problem, we use the sedimentation rate (0.22 cm/yr) obtained from $^{137}$Cs and the nuclear bomb $^{14}$C signal results for the upper 13 cm part. The Bacon mean age of 14-16 cm depth is −8 cal yr BP (1958 CE) which is very reasonable. If we artificially set up the age of 18-20 cm depth as 1950 CE, there would be sedimentation gap between 19 cm and 21 cm depths. Currently, we do not have evidence for supporting this change. Thus, we decided to adopt the Bacon mean age below 15 cm depth (thick black line in Fig. 4B). The core covers a continuously depositional history since 200 CE (1760 cal yr BP to the present).

### 4.4. TOC and TN results measured by EA

A total of 32 acid (0.5N HCl) leached samples were measured for TOC and TN in the sediments by EA. Variations of TOC, TN and C/N are plotted in Fig. 5. The average and standard deviation (n = 32) of TOC and TN are 17.1 ± 5.0% and 1.4 ± 0.5%, respectively. The TOC and TN values have a strongly positive correlation ($R^2$ = 0.92), indicating the two elements have the same source. The lake sediments contain relatively high organic carbon, ranging from 9.64% to 24.52%, which is much higher than soil TOC (normally <5%), implying that the lake productivity has been relatively high. The atomic C/N ratio has an average of 12.6 ± 1.7 (n = 32), ranging from 9.23 to 15.75. Fig. 5c and d shows the variations of TOC, TN and C/N. General increasing trends in TOC and TN but decreasing trend in C/N can be observed from the bottom (early time) to the top (modern time) of the core.

### 4.5. Elemental results measured by ICP-OES

As aforementioned, 0.5N HCl leaching fraction (AL) contains elements that are dissolved from carbonates, dissolvable oxides (e.g., $Al_2O_3$, $MnO_2$, $Fe_2O_3$, $Fe_3O_4$, etc.), particle and porewater absorptions. Unlike elemental contents measured by XRF, or ICP-OES/ICPMS measurement of the solutions treated by total dissolution of microwave digestion (close digestion) and Aqua Regia dissolution (open digestion), those AL elements can sensitively reflect lake chemistry changes under the influences of varying factors such as changes in productivity, redox conditions, pH, temperature, salinity, surface runoff. On the other hand, Aqua Regia (AR) dissolved elements account for >80% of the measured elements in the sediments (Engstrom and Wright, 1984; Koinig et al.,

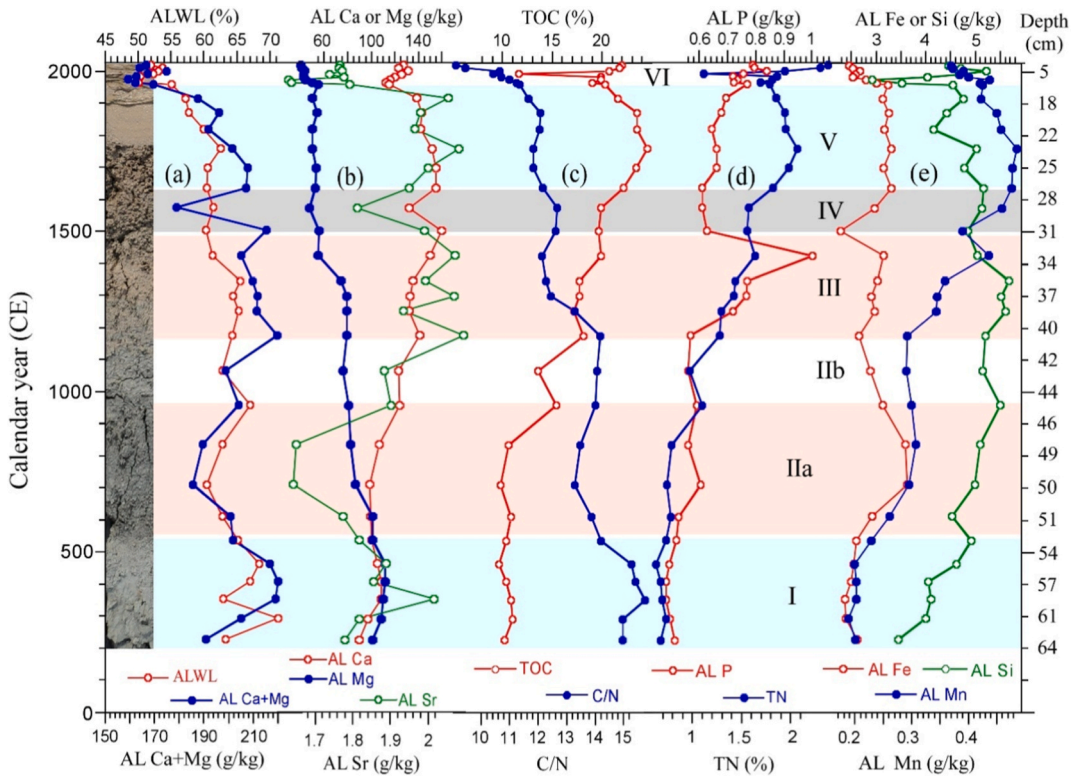


**Fig. 5.** Elemental profiles which show major variations in lake chemistry and productivity. Note that different elements have different units. The core is subdivided into six zones based on sedimentary features, geochemical proxies and pollen assemblages.

2003; Smrzka et al., 2019). Those elements come not only from authigenic minerals (such as carbonates and oxides) in the lake but also from terrestrial inputs including detritus. Thus, the AR elements should have higher concentrations than those of AL elements in the same sample, the formers contain more information about the input of terrestrial materials to the lake. In this study, we have conducted analyses of elemental concentrations in both AL and AR fractions from the same sediment sample. All the AL and AR elements of each sample were separated runs

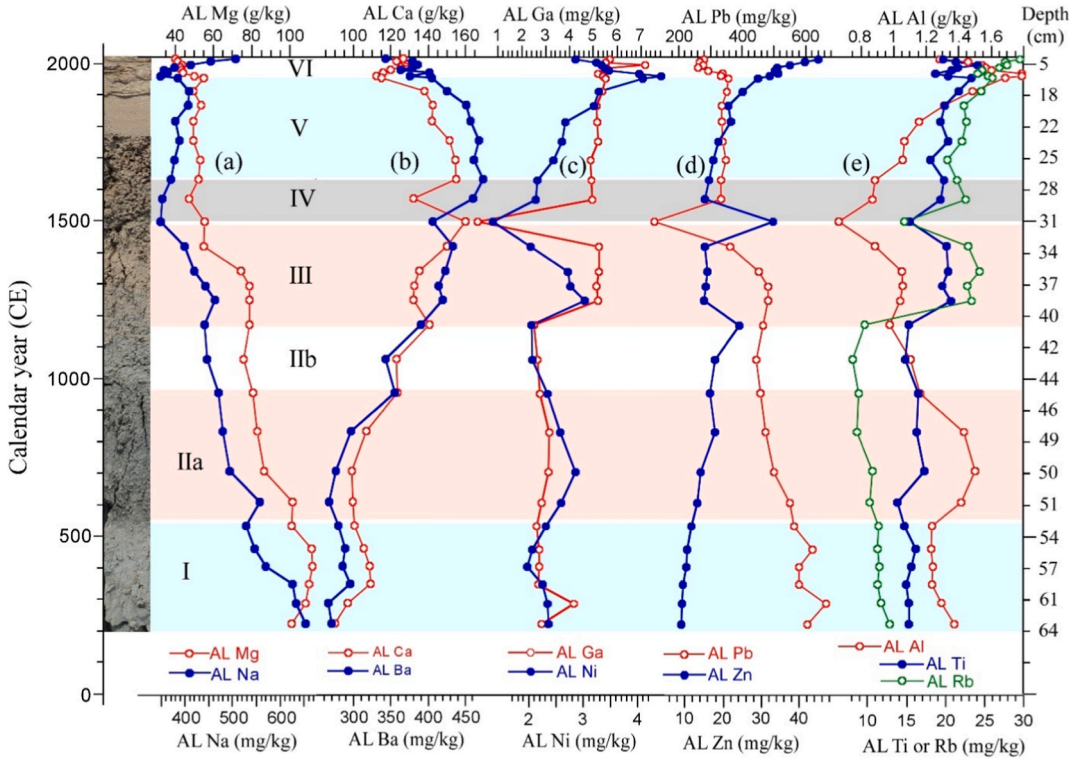


**Fig. 6.** Elemental profiles which reflect surface runoff and pollution to the lake. Note that different elements have different units.

from original sediment samples and were the absolute concentration in dry sediments (mg/kg). Here, we shall compare the elements of the AL solution and AR solution from the same samples.

Figs. 5 and 6 show the variations of selected elemental concentrations. We have calculated the average values of ALWL% and ARWL% as well as the average percentages of each measured element in AL phase vs. AR phase. The calculated results are listed in Table S2. Based on the measured 32 samples, the average acid leach weight loss (ALWL) and Aqua Regia dissolution weight loss (ADWL) are 60.4 ± 5.7% and 72.9 ± 3.1%, respectively (Table S2), indicating high carbonate content of the sediments as 60% of the samples can be dissolved by 0.5N HCl. The sediments contain ~27% detritus which cannot be dissolved by Aqua Regia. Those undissolved residues are mainly quartz and clay minerals such as Illite and Talc. XRD analysis of the samples will show these AR undissolved minerals in the next section.

The average concentrations of the 32 AL samples have the order of AL Ca (122,630 mg/kg) > Mg (68,900) > Si (4680) > Fe (2882) > Sr (1872) > Al (1264) > P (655) > K (640) > Na (450) > Pb (412) > Ba (373) > Mn (352) > Cu (40) > Zn (21) > Rb (19) > Ti (18) > U (14) > Ga (4.3) > Ni (2.7) > Cr (2.3) > Mo (1.3). Ca and Mg are the two highest elements in the AL fraction. Ca, Mg and Sr are earth alkaline elements, and precipitate with carbonates in natural water when pH reaches >7, agreeing with the high ALWL value. Fig. 5a displays good co-variance between ALWL and Ca + Mg ($R^2 = 0.73$). However, AL Ca and AL Mg do not have an apparent correlation ($R^2 = -0.4$) (Fig. 5b), implying carbonate minerals such as calcite ($CaCO_3$) and dolomite ($MgCa(CO_3)_2$) were dominant in different periods.

The average concentrations of the 32 AR samples are in the order of AR Ca (145,973 mg/kg) > Mg (61,940) > Al (7466) > Fe (7348) > Sr (2293) > Si (1565) > P (1427) > K (1116) > Na (697) > Ba (464) > Mn (401) > Ti (299) > Pb (189) > Cu (71) > Rb (64) > Zn (36) > Ni (33) > Ga(29) > U (28) > Cr (24) > Mo (7.6). Using AL and AR concentrations, we can calculate the AL/AR ratios for each element of the samples (Table S2). The AL and AR ratio listed in Table S2 should not exceed 100% because Aqua Regia is a much stronger acid than 0.5N HCl. The AL/AR ratio of Si and Pb are greater than 100%, indicating these two elements were partially lost during the AR dissolution. Although no HF was added during the AR digestion, $SiF_4$ could form during the digestion because F existed in the sediments such as Thomsenolite ($NaCaAlF_6 \cdot H_2O$), Karasugite ($SrCaAl(F, OH)_7$) and Polylithionite ($KLi_2Al(Si_4O_{10})(F, OH)_2$). Since our microwave digestor was broken, the open AR dissolution under 95°C overnight could allow $SiF_4$ degassing and causing Si loss. Pb, on the other hand, could form volatile compounds during the digestion under high temperature and prolonged heating. The AL/AR ratio of Mg is 110 ± 11% which is close to 100% within the uncertainty. This ~100% ratio indicates that most of Mg comes from carbonates. No Mg loss occurred during the AR digestion. However, as the concentration of Mg is quite high and oversaturated for

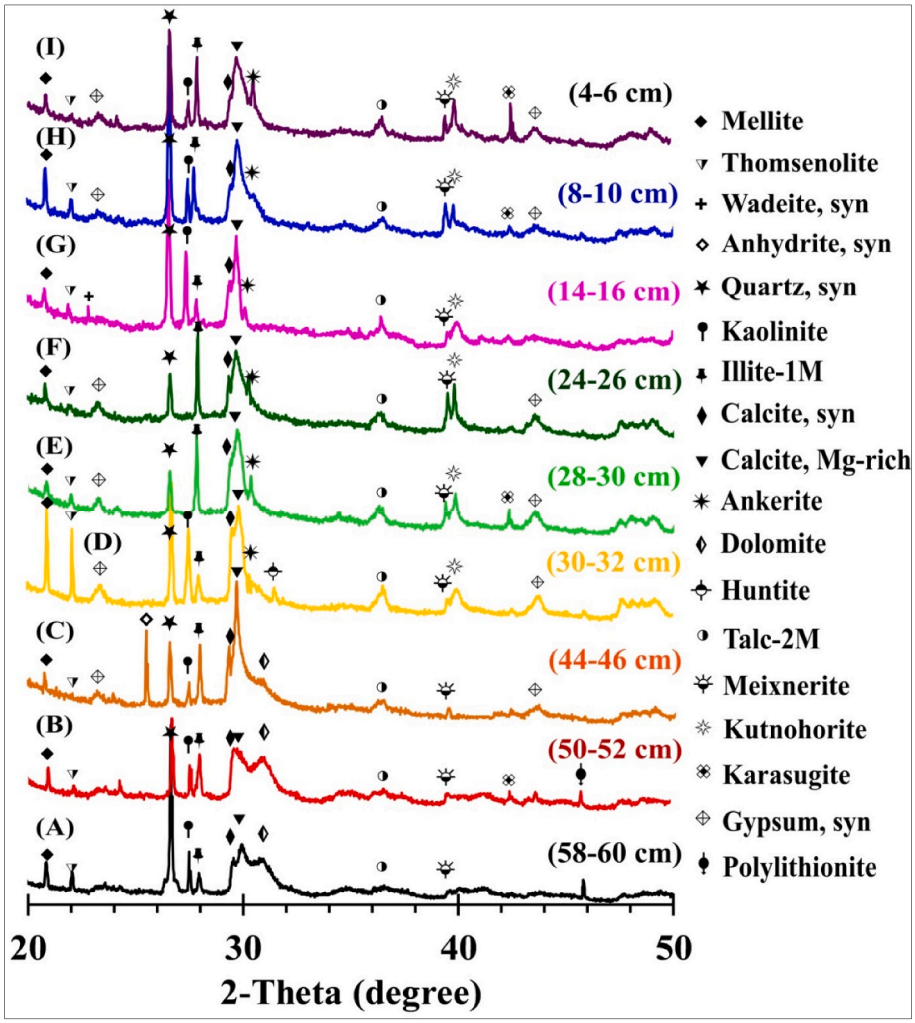


**Fig. 7.** Identified mineralogical compositions of the sediments from nine layers in Core 22-Al-03A using XRD analyses. These nine layers involve all zones except Zone III. Note that the peak height of minerals in each spectrum represent relative intensity, not the absolute content. The comparison of the peak height of other minerals with the quartz in a certain spectrum reflects the relative contents of the mineral in the sample.

the ICP-OES, the sample solution was diluted 20 times. The uncertainty of the analysis was probably increased due to the dilution. In a word, the AR Si and AR Pb are not reliable due to their loss during the AR digestion.

### 4.6. Mineral compositions of the lake sediments determined by XRD and SEM

Nine horizons (4-6, 8-10, 14-16, 24-26, 28-30, 30-32, 44-46, 50-52 and 58-60 cm) from the core were selected for XRD and SEM analyses. Fig. 7 shows the XRD spectra. The chemical compositions of the 9 samples are listed in Table S3, and the SEM micrographs are shown in Fig. S3 in the supplement materials. The identified minerals are classified into 12 groups according to Dana's classification (Gaines et al., 1997) as: Carbonates including Calcite, Calcite Mg-rich, Ankerite ($CaFe(CO_3)_2$), Dolomite, Kutnohorite ($Ca(Mn,Mg,Fe)(CO_3)_2$), and Hunite ($CaMg_3(CO_3)_4$); Clay minerals including Talc, Illite, and Kaolinite; Halides including Thomsenolite and Karasugite; Hydroxides including Meixnerite; Organics including Mellite; Oxides including Quartz; Sulfates including Gypsum and Anhydrite; Silicates including Polylithionite.

The SEM imagines shown in Fig. S3 exhibit calcite, Mg-calcite and dolomite crystals, supporting that carbonates are dominant minerals measured by XRD. In addition, the chemical compositions measured by EDX-SEM listed in Table S3 agree with Ca and Mg concentrations determined by ICP-OES not only in relative contents but also in variation trends (Fig. S4). While the elemental concentrations determined by ICP-OES provide high-resolution changes in the lake chemistry (AL fraction related: pH, salinity, alkalinity and redox conditions) and productivity (organic proxies) as well as in terrestrial input (AL fraction related: detrital input), mineral compositions of the nine horizons determined by XRD give insights on sedimentary changes.

### 4.7. Pollen results

Palynomorphs in lake sediments include tree, shrub and herb pollen taxa, as well as remains of algae, fungi and invertebrate, which reflect past climatic conditions such as air temperature, precipitation, atmospheric circulation and solar activity, as well as human influences on vegetation cover, sedimentary input and farmland development (Bennett and Willis, 2001). The selected major pollen taxa are presented on Fig. 8. The revealed pollen assemblages were subdivided into four pollen zones (PZ).

PZ I (64-45 cm, ~200-960 CE) was characterized by the predominance of AP, although NAP (mainly Amaranthaceae) demonstrates a gradual increase in the upper part of the zone (52-45 cm). The pollen concentration was low (up to $3 \times 10^5$ grains/g) at the bottom part of the zone, but it increased sharply (up to $13 \times 10^5$ grains/g, 48-46 cm) in the upper part of the zone. Among non-pollen palynomorphs (NPP), there was a rise in the content of saprotrophic and coprophilous fungal spores in the upper part of the zone with a simultaneous decrease in green algae remains (*Pediastrum*).

PZ II (45-35 cm, ~960-1350 CE) showed a sharp increase in *Artemisia,* Poaceae pollen percentages, and in pollen concentration (up to $4.0x10^5$ grains/g), while Amaranthaceae pollen contents decreased. The contents of *Pediastrum* remains were higher in this zone than the PZ I.

Pollen concentration increased in PZ III (35-21 cm, ~1350-1820 CE) up to $13.2 \times 10^5$ grains/g. In the upper part of the zone, *Pinus* and Amaranthaceae pollen percentages decreased, while the contents of *Artemisia* rose. The lower part of the zone *Pediastrum* remain contents sharply increased (with maximum value in 28 cm), while saprotrophic, coprophilous fungal spore contents declined in the upper part of the zone.

PZ IV (21-0 cm, ~1820-2022 CE). This zone is notable for the increase in pollen concentrations (up to $16 \times 10^5$ grains/g) accompanied by a change in the dominant pollen taxa. The *Pinus* pollen percentages decrease, while the *Betula* sect. *Albae*-type pollen contents gradually increase. Among herbaceous pollen taxa *Artemisia* (maximum value at 18 cm), Amaranthaceae, Cyperaceae (maximum value at 14 cm), and Poaceae are most abundant. Generally, NAP contents reach 59%, while the AP contents decrease to 41%. In the middle part of the zone (14-10 cm), there is a peak in the saprotrophic, coprophilous and parasitic

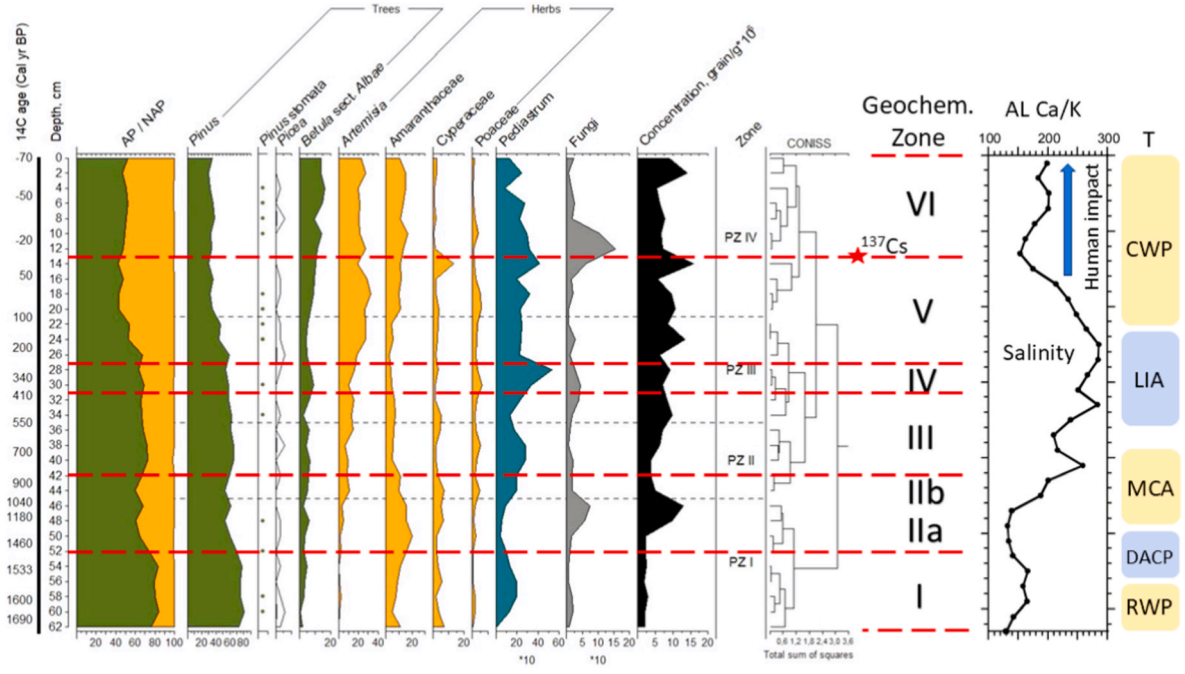


**Fig. 8.** A pollen diagram of the core 22-Al-03A with selected palynomorphs and its comparison with geochemical zones. The pollen zones are divided by the black dashed lines. The last column on the right side shows the six geochemical zones which are separated by the red dashed lines. The red star denotes the depth of the $^{137}Cs$ peak which reflects the deposition at 1963/64 CE. AL Ca/K representing lake salinity and climatic episodes are added on the right side for comparison. RWP, DACP, MCA, LIA and CWP denote Roman Warm Period, Dark Ages Cold Period, Medieval Climate Anomaly, Little Ice Age and Current Warm Period, respectively.

fungal spores. The presence of *Pediastrum* remains gradually decreases upwards.

## 5. Discussion

### 5.1. Geochemical variations and zones based on elemental and mineral analyses

Organic matter in lake sediments is an important indicator of lake productivity and carbon source. The TOC, TN and C/N of lake sediments are paleoclimatic and paleoenvironmental proxies, as they are functions of lake productivity, oxidation condition and surface runoff (Kaushal and Binford, 1999; Perdue and Koprivnjak, 2007; Gälman et al., 2008; Kasper et al., 2013; Lone et al., 2018; Han et al., 2022; Misra et al., 2025). In general, higher lake productivity, reduced condition (lower redox value) and lower surface runoff will result in higher TOC and TN but lower C/N ratio. TOC in lake sediments can come from organic composition of both plants and organisms, while TN under natural condition is mainly from organisms formed in lake water, so that higher TN but lower C/N indicate more organic matter generated in the lake (Li et al., 2016b; Dong et al., 2018). In addition, high surface runoff would bring more terrestrial materials which have higher C/N of organic matter into the lake sediments, resulting in higher C/N. Furthermore, wet climates produce higher runoff which lead to decrease in nutrient concentration and productivity in lake water (Yang et al., 2021). Lower redox condition is in favor of organic preservation. Using the variations of TOC, TN and C/N shown in Fig. 5c and d, we are able to interpret the lake productivity and exogenous/endogenous organic matter (OM), with higher TOC and TN but lower C/N ratio indicating higher lake productivity in the lake, and vice versa. Low TOC and TN with relatively high C/N below 49 cm depth (before 850 CE) reflect low lake productivity and high surface runoff (more exogenous OM) under cold and wet conditions (Fig. 5c and d). The TOC and TN continuously increased from 850 CE to their maximum values until 1750 CE, then slightly decreased to 1964 CE. Both TOC and TN had a sudden and strong drop at 1990-1991 CE, which might indicate an event associated with human activity. Following this event, both TOC and TN have sharp increasing trends. The lake productivity referred by the increased TOC and TN trends between 850 and 1750 CE could not be simply explained by temperature or precipitation alone because both warm (MWA) and cold (LIA) conditions were involved in this period. On the other hand, C/N was significantly lowered between 1200 and 1300 CE, then continuously dropped from 1870 CE. In order to understand the lake history, elemental geochemistry should be used.

For the 21 elements analyzed by ICP-OES, they can be classified into several groups: (1) earth alkaline elements (Ca, Mg and Sr) are mainly in carbonates; (2) alkaline metal elements (K and Na); (3) detrital elements (Al, Si, Ti, Ba); (4) oxide elements (Fe, Mn); (5) heavy metal elements (Cu, Ni, Zn, Cr, Ga, Pb); (6) trace metal elements (U, Rb, Mo); and (7) biogenic element (P). The AL fraction concentration of the elements reflects its authigenic origin which is strongly affected by lake water chemistry, temperature, pH and redox conditions, whereas the AR fraction concentration of the elements indicates total concentration including both authigenic origin and terrestrial input. Based on the AL and AR concentration variations of the samples (Figs. 5 and 6), we shall discuss changes in the lake chemistry and input materials throughout the core.

In Figs. 5 and 6, the selected major geochemical proxies (TOC, TN, C/N, AL and AR elements) were plotted against chronology. Based on the geochemical variations, six zones can be classified as follow.

Zone I (64-52 cm, ~200-570 CE): the sediment was grey-blue clay without plant remains. The lowest TOC and TN but highest C/N, lowest acid-leachable (AL) Fe and Mn but highest AL Mg and Na reflected high terrestrial surface runoff due to glacier melting and low lake productivity in cold and fresh lake water. Although Mg was the highest in this zone, Mg came chiefly from dolomite which normally forms in high pH, warm and saline water such as marine environment. Thus, the high dolomite and Mg probably reflected weathering of bedrock in the study area. When the lake had low salinity, pH and productivity, low calcite percentages and low Ca concentrations were recorded. Fe and Mn stay in water under anoxic conditions, but precipitate as oxides in the sediments under oxic conditions. Hence, this zone revealed a fresh lake with low productivity and inputs of cold water under a wet climate.

Zone II (52-41 cm, ~570-1170 CE) can be subdivided in two subzones: IIa (52-45 cm, 570-960 CE) and IIb (45-41 cm, ~960-1170 CE). In Zone IIa, the color of the lake sediment became darker with more organic carbon (OC) produced in the lake. The lake productivity was still low in the fresh and oxic conditions shown by the lowest AL Sr but highest AL Fe under a warm and wet climate. In Zone IIb, strongly increased lake productivity and lower redox conditions shown by elevated TOC, TN, AL Sr and reduced AL Fe, corresponded to the warm climate of MCA.

Zone III (41-31 cm, ~1170-1500 CE): the lake became very productive with high salinity and oxic conditions shown by increased TOC, TN, AL P, AL Fe and Mn, AL Ca and Sr, but decreased C/N, perhaps under both climatic and anthropogenic influences. The color of the sediments turned to brown.

Zone IV (31-27 cm, ~1500-1640 CE): a sudden drop occurred in most geochemical proxies except AL Zn and organic matter probably corresponding to the cold climate during the beginning of the Little Ice Age (LIA). Carbonate precipitation in the cold water was reduced significantly. However, high lake productivity as indicated by TOC, TN and pollen results occurred during the warm season.

Zone V (27-13 cm, ~1640-1963 CE): the lake had very high productivity, salinity and alkalinity reflected by high values of TOC, TN, AL Ca, AL Sr, AL Fe and AL Mn. The lake chemistry and productivity during this period may have been strongly affected by human activities. At around 1958 CE the lake's chemistry and sedimentation was strongly influenced by human impact.

Zone VI (13-0 cm, ~1963-2022 CE): the sedimentation rate increased from <0.043 cm/yr in previous zones to 0.223 cm/yr in this zone due to farmland development near the lake (Fig. 1B–Andreenkov, 2021). From the 1960s until the 1980s, sharp decreases in AL Sr, Ca, Si, Fe and Mn concentrations were recorded. In contrast, strong increases occurred in Al, Ni and Zn concentrations, which might be related to pollution. Around 1991 CE, there was a sharp large drop in TOC and TN. Based on C/N, the organic matters are mainly generated inside the lake. This historic event was documented by local authorities. After 1991 CE, the lake recovered and stabilized to its modern status, i.e. a high productive and alkaline lake with anoxic conditions. The AL Pb concentrations in the core sediments are one order of magnitude higher than what is generally reported from lake sediments, which may be attributed to the high Pb background in the rocks of this area.

The mineral contents of the sediments generally agree with the elemental results of the core. Quartz and many clay minerals are present in the sediments, so that the residue of the AR open digestion is close to 27% (ADWL = 72.9%). Calcite and dolomite are major carbonates in the sediments, supporting high AL Ca, Mg and Sr. Dolomite, that is normally precipitated in high pH and saline water, appeared only in the depths below 44 cm (Fig. 7A and B). However, the lake was relatively fresh (low AL Ca) and had low productivity (low TOC) reflecting terrestrial input, so that the dolomite might came from surface runoff, which is supported by the highest C/N. The high terrestrial input is also supported by Polylithionite ($K(Li_2Al)Si_4O_{10}F_2$) which is visible only in Fig. 7A and B. On the other hand, calcite (Mg-rich) became clearly the dominant mineral in the sediments above the depth of 46 cm (Fig. 7C–I), indicating authigenic carbonate precipitated in the lake water. Anhydrite ($CaSO_4$) appeared only in the sample at 44-46 cm depth (Fig. 7C), implying warming and oxic (agreeing with the highest AL Fe) lake water. Mellite (also called Honeystone, $Al_2C_6(COO)_6{\cdot}16H_2O$) and Thomsenolite ($NaCaAlF_6{\cdot}H_2O$) had highest abundance (Fig. 7D). Mellite is a rare, naturally occurring organic mineral compound and Thomsenolite can be

converted from Cryolite ($Na_3AlF_6$) which is formed under cold temperature. Therefore, high contents of Mellite and Thomsenolite indicated that the lake water could be cold and organic rich corresponding to the beginning of the LIA. Accompanying Calcite and Mg-rich Calcite deposition, Ankerite (Fe- and Mn-dolomite) and Huntite ($CaMg_3(CO_3)_4$) became visible in the spectrum in Fig. 7D. This phenomenon may be explained by that increased solubility of Calcite in the cold water led to replacement of Ca with Mg, Fe and Mn in the carbonates. Kaolinite and Illite are clay minerals and come from detritus carried by surface runoff into the lake. In Fig. 7E and F, the spectra did not show Kaolinite in the period of 1550~1700 CE, probably reflecting that the weathering conditions were not in favor of Kaolinite. After 1958 CE, Kaolinite input to the lake was attributed to both climatic and human impacts.

### 5.2. Vegetation changes

Changes in pollen spectra reflecting vegetation and climatic changes in the study area over the past 1800 years can be interpreted as follow. Pine forest existed around the lake in the period 200-570 CE. Treeless vegetation with numerous amaranths was less common. Climate conditions were relatively cold.

Pollen spectra accumulated between 570 and 960 CE reflect that the pine forest around the lake was retreating somewhat and open herb communities with amaranth plants showed maximum distribution around 660 CE. *Pediastrum* content was the lowest, which may point to the disappearance of shallow water habitats in the lake. The climate during this period became somewhat drier.

Pollen spectra from the sediments accumulated between 960 and 1350 CE revealed changes in steppe communities as wormwood and Poaceae taxa became more widespread, while participation of amaranths decreased. These changes reflect that climatic conditions were slightly more humid during this time interval coinciding with the MCA.

Forest and steppe communities dominated around the lake between 1350 and 1730 CE. The lower amounts of amaranth pollen in the sediments document a reduction of amaranth in the local vegetation pointing towards increased moisture.

The uppermost pollen assemblages document that pine forest retreated and herb communities with wormwood and amaranth were developed around the lake during the last 160 years. These changes and spread of birch from 1860 CE were probably due to anthropogenic influence. The climatic conditions became warmer and drier. Saprotrophic, coprophilous and parasitic fungal spores in the sediments peaked between 1958 and 1970 CE indicating further anthropogenic impact on the study area during the agrarian reforms (Andreenkov, 2021; Fedorova and Manchenko, 2022).

### 5.3. Combing elemental geochemical, mineralogical and pollen records of the core

The above classification and description about the pollen zonation have some discrepancies from the geochemical zones (Fig. 8). The possible explanation is that geochemical changes in the lake occurred much faster and more sensitively to climatic changes, while changes in local vegetation reflected in pollen spectra show some delay. Therefore, the changes in the lake chemistry reflected by the geochemical zones better reflect change in climatic conditions than changes of local vegetation.

We added geochemical zones to pollen zonation on Fig. 8 for comparison. PZ I covers Zone I and most of Zone II; PZ II includes the upper part of Zones IIb and lower part of Zone III; PZ III includes the upper part of Zone III, Zone IV and lower part of Zone V; and PZ IV involves the late half of Zone V and Zone VI (Fig. 8). The pollen zonation was determined by many pollen taxa and classified by computer software. It is notable that pollen zonation has a decadal-to-centennial time-leg in comparison to the geochemical zonation. However, there are some changes in major pollen taxa contents which were not identified into the pollen zonation. For instance, the low part (62-52 cm) of PZ I was significantly different from the upper part (52-35 cm) of PZ I in terms of AP/NAP, Amaranthaceae and fungal spore percentages, as well as in pollen concentration. It is likely that the pollen assemblage between the geochemical Zones I and II could not be differentiated in the CONISS zonation. Below we point out the major features of pollen records with climate significance in each geochemical zone (Fig. 8).

In Zone I, the AP/NAP was the highest, but *Artemisia*/Cyperaceae (A/Cy) ratio was the lowest (Fig. 8), indicating that the climatic conditions were rather cold and wet that agree well with fresh water and cold lake conditions reflected by low bioproductivity and by geochemical proxies.

In Zone IIa, the AP/NAP ratio decreased, while pollen concentration significantly increased. Amaranthaceae pollen contents are maximal and contents of *Pediastrum* remains are minimal in this zone. These changes in pollen assemblages indicated that the climatic conditions were warmer and drier than those in Zone I, but cooler and wetter than the modern climate. The geochemical proxies in Zone IIa zone also suggest a lake with low salinity, productivity, redox conditions (low oxic) and with reduced surface runoff. In Zone IIb which coincides with the MCA, the pollen assemblages showed increased lake productivity (increased presence of *Pediastrum* remains) under a warmer (increased *Artemisia*/Cyperaceae)/drier (decreased AP/NAP) climate. The AP/NAP ratio (Fig. 8) is relatively constant through Zones III and IV, but slightly higher than that during Zone II and significantly lower than that during Zones IV and V, reflecting the regional MAP was the highest in Zone I, dropped to a lower but unstable level in Zone II, then slightly elevated to a stable level in Zones III and IV, and further declined to relative stable level in Zones V and VI. Based on the AP/NAP, we may assume that the regional MAP over the past 1800 years shows a decreasing trend. On the other hand, the A/Cy ratio (Fig. 8) shows an increasing trend from Zone I toward to Zone VI, reflecting the MAT increasing trend over the past 1800 years. The major differences in pollen assemblages between Zone III and Zone IV are the highest contents of *Pediastrum* remains in Zone IV (~1500-1640 CE, early LIA).

Previous studies showed that changes in the taxonomic composition of *Pediastrum* can be used as an indicator for temperature change (Turner et al., 2016; Xiang et al., 2021), and *Pediastrum* body size is also a function of water temperature due to longer and faster growth in warmer water (Huang et al., 2023). Unfortunately, in this study, we have only *Pediastrum* abundance without information of taxonomic composition and body size of *Pediastrum*. Assuming that the *Pediastrum* abundance in Fig. 8 is related to the lake water temperature, salinity and nutrient concentration (Xiang et al., 2021 and references therein), we may discuss the significance of *Pediastrum* abundance. In Fig. 8, AL Ca/K variation is added for representing lake salinity change with warm/cold climatic episodes on the right side. It seems that *Pediastrum* abundance correspond to higher lake salinity and nutrient concentration (higher lake TOC) but not to higher water temperature. For instance, during cold LIA the *Pediastrum* abundance was high. Generally, cold climate could result in low lake productivity and salinity, however, the geochemical proxies indicate that the lake productivity and salinity was not low with high AL Ca/K ratio and TOC% (Figs. 5 and 8). Thus, the controlling factor for the lake productivity and salinity might not be water temperature. If the climatic conditions during the cold LIA were dry, the lake body became smaller with less surface runoff, the lake salinity and nutrient concentration could increase to generate moderate lake productivity during the warm season. Therefore, the climatic conditions during the LIA should be cold and dry.

We may summarize that changes in the pollen assemblages demonstrate a decadal-to-centennial time lag compared to the changes in the geochemical curves, as the geochemical proxies are more sensitive to local climatic changes. Nevertheless, many fluctuations in the revealed pollen assemblages agree well with the geochemical features of the lake sediments. Hence, the geochemical proxies are favorable to reconstruct rapid climatic change on local scale, whereas the pollen proxies are better for vegetation reconstruction under regional scale, with NAP and

algae abundance reflecting mainly local environments.

### 5.4. Paleoclimate and paleoenvironment over the past 1800 years based on the Zolotoe record

The 22-Al-03A core record from Zolotoe Lake covers the past 1800 years, which include three warm periods (RWP, MCA and CWP) and two cold periods (DACP and LIA). It is worth mentioning that temperatures recorded in Europe during the period 450-800 CE were particularly cold, so that the period was named the Dark Age cold Period in the literature. In China, however, many records indicated warm and wet climate conditions during 550-780 CE (e.g., Ge et al., 2017). The pollen-based temperature reconstruction from Lake Teletskoye (51°35′N, 87°40′E) in Russian Altai, also indicates relatively warm conditions during 750 to 550 CE (1.4-1.2 cal yr BP) (Rudaya et al., 2016). Hence, temperature during part of the DACP (550-780 CE) was not particularly cold. Nevertheless, based on the sedimentary feature, geochemical proxy, pollen assemblages and mineral composition of the lake sediments, we can evaluate how these global climatic intervals were recorded in the study area.

Fig. 9 shows the main variations of the sedimentary, geochemical and pollen proxies with depths, ages and zones. The sedimentation rate (SR) was below 0.05 cm/yr prior to 1958 CE, then rose to 0.3 cm/yr. This sudden SR increase is caused by human activity, due to more intensive farmland development since the 1930s (Andreenkov, 2021). In Fig. 9a, variations of TOC and C/N indicate lake productivity and exogenous/endogenous carbon source, with higher TOC and C/N reflecting higher productivity and higher exogenous/endogenous ratio, and vice versa (Meyers and Ishiwatari, 1993; Bridgham and Richardson, 2003). Unlike Figs. 5 and 6, Fig. 9 shows some elemental ratios instead of elemental concentrations against ages, as the elemental ratios are more robust indicators than concentrations, as these can be affected by mineral contents from terrestrial inputs that obscure the influence of lake chemistry.

Fig. 9b exhibits the variations of AL Sr/Ca, AL Ca/K and AL Al/Ti. In general, Sr/Ca, Mg/Ca and Ca/K ratios are often used for indication of lake salinity change, with higher Sr/Ca, Mg/Ca and Ca/K reflecting higher lake salinity; and vice versa (Li et al., 2000, 2004; C.J. Zhang et al., 2020a,b; Misra et al., 2025). Because aragonite, Mg-calcite and dolomite indicate high pH, temperature and water salinity, higher Sr/Ca and Mg/Ca indicate higher salinity. However, when dolomite and Mg-calcite come from terrestrial input, then Sr/Ca and Mg/Ca ratios may not reflect the lake chemistry. On the other hand, Ca/K can serve as an indicator of lake salinity due to $CaCO_3$ precipitation when salinity increases. In general, higher Ca/K indicates higher salinity (Barjaktarovic and Bendell-Young, 2002; Liang et al., 2024). If all three ratios of Sr/Ca, Mg/Ca and Ca/K in Zolotoe Lake sediments represent salinity change, then they would have similar trends. However, AL Sr/Ca has opposite trends with AL Ca/K in Fig. 9b. The correlation between AL Sr/Ca and AL Mg/Ca is quite strong ($R^2 = 0.89$) in Core 22-Al-03A, indicating both Sr/Ca and Mg/Ca ratios are controlled by the carbonate minerals which are influenced by terrestrial input. The XRD results shown in Fig. 7 illustrated that the dolomite in the deeper layer in the core came from surface runoff. Therefore, Sr/Ca and Mg/Ca ratios in the core could not be indicator of the lake salinity. In fact, Sr/Ca has a similar trend with AL Al/Ti in Fig. 9b, the latter is an indicator of terrestrial input. Higher Al/Ti ratios generally suggest increased surface runoff and sediment transport into the lake, while lower Al/Ti ratios may indicate periods of reduced runoff or sediment input. Although both Al and Ti are considered terrigenous (originated from land rather than the lake itself), Ti tends to be preferentially removed from sediments compared to Al, so that sediments transported by surface runoff and

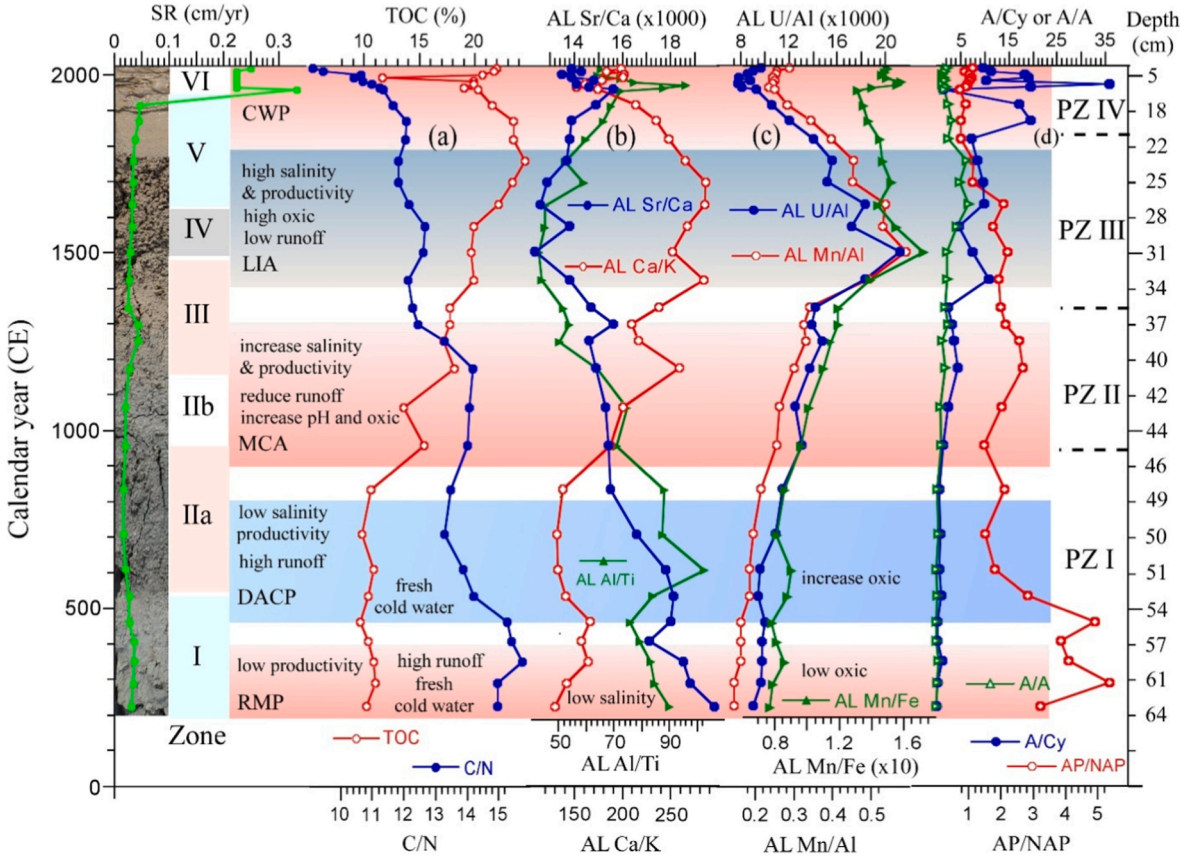


**Fig. 9.** A summary figure with the sediment photo, sedimentation rate, geochemical zone and major geochemical proxies, major pollen zone and proxies. (a) TOC and C/N; (b) AL Sr/Ca, AL Ca/K and AL Al/Ti; (c) AL U/Al, AL Mn/Al and AL Mn/Fe; (d) AP/NAP, A/Cy (*Artemisia*/Cyperaceae) and A/A (*Artemisia*/Amaranthaceae).

deposited in the lake will show a higher Al/Ti ratio than the original source material due to the preferential removal of Ti (Bertrand et al., 2024). Thus, the AL Sr/Ca and Mg/Ca ratios in the 22-Al-03A core do not reflect salinity change; they are function of surface runoff, with lower ratios indicating lower surface runoff similar to the AL Al/Ti ratio (Fig. 9b). In contrast, Ca/K in the core is an indicator of the lake salinity, with higher ratio reflecting higher salinity.

The variations of AL Mn/Fe, AL Mn/Al and AL U/Al are shown on Fig. 9c. All three ratios were considered as indicators of redox conditions, with higher Mn/Fe and Mn/Al ratios and lower U/Al ratio reflecting more oxic (oxygen-rich) conditions (Scholtysik et al., 2022; He et al., 2023; Swanson et al., 2023). In Fig. 9c, all three ratios have similar trends, and the correlation between AL Mn/Al and AL U/Al is quite high ($R^2 = 0.79$). The positive correlation between AL Mn/Al and AL U/Al points out that AL U/Al in the core should not be an indicator of redox conditions because higher AL Mn/Al reflects more oxic conditions whereas higher AL U/Al implies more anoxic conditions. In fact, in Core 22-Al-03A the average AL Mn is 352 ± 94 mg/kg which is much higher than that of AL U (14 ± 2 mg/kg), and the average AL/AR Mn is 87.1 ± 13.9%. This means that most Mn in the sediments is dissolved by 0.5N HCl, and the Mn is mainly in authigenic minerals (e.g., $MnCO_3$, $MnO_2$) formed in the lake. U (VI) is likely scavenging with Mn minerals in the lake. Besides, $Al_2O_3$ may precipitate prior to $MnO_2$ when the lake pH increases, so that both Mn and U co-precipitate with $Al_2O_3$, leading the positive correlation between AL Mn/Al and AL U/Al. Hence, in Zolotoe Lake AL Mn/Al may be a function of redox conditions and pH, with higher Mn/Al reflecting higher pH and more oxic conditions; whereas AL Mn/Fe is more sensitive to redox conditions, with higher ratio indicating more oxic conditions.

Fig. 9d plots the profiles of AP/NAP, A/Cy (*Artemisia*/Cyperaceae) and A/A (*Artemisia*/*Amaranthaceae*) throughout the core. As mentioned earlier, AP/NAP may have positive relationship with MAP, and A/Cy and A/A may have positive relationship with MAT. By comparison with the A/A variation, the A/Cy variation is much larger and more sensitive to climatic changes. The A/Cy values during the LIA were higher than those during the earlier periods. This observation does not agree with the positive relationship with MAT. Thus, the A/Cy must be influenced by other factors. The A/Cy variation trend was similar to the trends of TOC and AL Ca/K before 1820 CE, implying that increased salinity of the lake would provide higher lake productivity and more *Artemisia* content; and vice versa. Human impact after 1820 CE might disrupt this relationship. A reasonable explanation of the positive relationship among A/Cy, salinity (AL Ca/K) and productivity (TOC%) is that reduced input water (decreases in AL Al/Ti and AL Sr/Ca) under dry climate would elevate lake salinity and nutrient concentration due to evaporation, so that lake productivity was enhanced. Therefore, A/Cy ratio should be also affected by moisture conditions beside air temperature. Fig. S5 shows the comparison of A/Cy with the air temperature and precipitation recorded in Barnaul Meteorological Station since 1838 CE. The comparison illustrates that higher A/Cy ratio corresponded to higher precipitation on decadal or shorter time scales. The long-term temperature increasing trend since 1830s is not clearly shown in A/Cy trend. Thus, hydroclimatic condition should be a factor to influence A/Cy ratio in lake sediments.

AP/NAP variations shown in Fig. 9d exhibits a general decreasing trend: 2.8-5.4 between 200 and 540 CE, 1.4-2.1 - during ~610-1070 CE, 1.1-2.7 - during ~1070-1700 CE and 0.7-1.1 - during ~1700-2022 CE. If the AP/NAP had positive correlation with MAP, the trend would mean that climate conditions became drier starting from 200 CE. However, other proxies do not confirm this. Thus, AP/NAP ratio should be affected by some other factors besides the precipitation. It is also notable that the AP/NAP was the highest in Zone I (Fig. 8), although the pollen concentration was the lowest. In general, the wetter climate conditions are favorable for vegetation development, which would be reflected in the higher pollen concentration. The geochemical proxies in Zone I support the cooler and wetter conditions, reflected by the lowest TOC, low salinity (AL Ca/Ka), high surface runoff (AL Al/Ti) and low oxic conditions. However, the NAP contents increased significantly after 600 CE as reflected by the reduced AP/NAP ratio and this coincided with a period of lower salinity, pH, temperature and nutrient level in the lake. From this, we deduct that the AP/NAP ratio in the Zolotoe Lake pollen record cannot be considered as a reliable MAP indicator.

Combining sedimentary feature, geochemical proxies, pollen assemblages, mineral information, we can reconstruct climatic conditions in the study area over the past 1800 years. The lake had low productivity (low TOC), low salinity (low AL Ca/K), low oxic condition (low AL Mn/Al and AL Mn/Fe), but high surface runoff (high AL Al/Ti, AL Sr/Ca, C/N ratios) under cooler and wetter climate conditions during ~200-800 CE. However, the Ca/K was slightly increased during the RWP (~200-400 CE), reflecting an increase in the lake salinity probably under the drier and warmer climate. The warming condition could have caused glacier melting and lead to increased inputs of cold and fresh water to the lake. According to previous studies on glaciers in the Russian Alai Mountains, three glacier advances were recorded over the Holocene: Akkem Stage (4900–4200 yr BP), Historical Stage (2300–1700 yr BP) and LIA or Aktru Stage (13th–19th centuries). During the RWP (ca. 250 BCE–400 CE), MCA (ca. 950–1250 CE) and CWP (1800 CE–present), the Altai glaciers retreated, especially after 1950 CE (Agatova et al., 2012; Solomina et al., 2016; Ganyushkin et al., 2022).

The geochemical proxies (Figs. 6 and 9) point to the cooler and wetter climatic conditions during the DACP (~450-800 CE), and the minimum abundance of *Pediastrum* also indicated low salinity and nutrient concentration. But, the strong decreases in AP/NAP and C/N during the DACP reflected that not only aquatic plants were developed surrounding and inside the lake, but also a retreat of forest occurred in the area. The climatic conditions in the study area became warmer and relatively wetter as reflected by increases in TOC, AL Ca/K, AL Mn/Al, AL Mn/Fe, AP/NAP ratio increase in pollen concentration, and stable C/N at high level between ~850 and 1200 CE. Higher temperatures elevate the lake productivity, salinity and oxic conditions.

The climate conditions during MCA (~900-1300 CE) in the study area was probably not as wet as during the RWP and DACP. At the end of MCA (~1200-1300 CE), the climate became warm and drier.

From 1300 to 1800 CE, the major features of the Zolotoe Lake environment were increasing salinity and bioproductivity, low surface runoff (minimum runoff shown by AL Al/Ti curves), maximum oxic condition, and increased A/Cy and A/A. The revealed changes were attributed to drier, but not to warmer climatic conditions during this period. When evaporation is higher than precipitation during the cold intervals like the LIA, elevated nutrient concentration caused by evaporation would result in high lake productivity. Our reconstruction coincides well with the temperature record in Barnaul Meteorological Station since 1838 CE and demonstrates that temperature during the LIA was about 3-4$^{o}$C colder than the present (Fig. S2). We assume that climatic conditions in the study area during the LIA were colder and drier than modern ones.

Another scenario could have happened in Zolotoe Lake in relation with the evolution of the Volchikhinsky lake system (Fig. 1). During the RWP and DACP, wetter climate resulted in a large lake system connecting the lake bodies in the Volchikhinsky lake system. The lake water was cold and fresh with low bioproductivity. Since the MCA, warmer climate caused stronger evaporation and reduced the water volume in the Volchikhinsky lake system. The drier climate conditions during the LIA have further caused the disappearance of the large lake system. Most likely, the Volchikhinsky lake system changed to a number of smaller lake bodies around 1600 CE as the lake sediments demonstrate increased TOC, maximum in salinity and oxic conditions, increased A/Cy and A/A, and decreased AP/NAP. Probably, after 1600 CE, Zolotoe Lake became an isolated water body, more sensitive to climatic changes and human influences.

Zolotoe Lake sediments accumulated between 1750 and 1950 CE show the decreases in TOC (productivity), salinity (AL Ca/K), oxic

conditions (AL Mn/Al and AL Mn/Fe) and increased surface runoff (AL Al/Ti). Human impact would not cause such geochemical shifts. The revealed changes suggest that the climatic condition was wetter during this interval. Higher aquatic plants and lake algae led to drop in C/N. After 1950 CE, the strong increase in the sedimentation rate (about 7 times) marks strong increase of human impact. However, climate influence on the proxies from the sediment core can also be documented in this interval by the peak of AL Al/Ti around 1973 CE, A/Cy peaks around 1973 CE and 1990 CE, the TOC trough around 1990 CE. These features might correspond to the high rainfall in the two intervals (Fig. 9 and S5).

### 5.5. Significance of the Zolotoe record in the regional context

Although Holocene paleoclimate records in Altai region including from the Russian, Chinese, Mongolian and Kazakh sides are abundant (e.g., Blyakharchuk et al., 2007, 2020; Liu et al., 2008; Rudaya et al., 2012, 2016; Jiang et al., 2013; Wang and Feng, 2013; Zhang et al., 2016; Huang et al., 2018; Karachurina et al., 2023), high-resolution records with robust chronology and multi-proxy for the past 2000 years are very limited. The Zolotoe Lake record from this study indicates that wet climates were prevailing during the RWP (warm/wet) and DACP (cold/-wet), and cold/dry climates were dominant in the early LIA (~1400-1750 CE) but at the end of LIA (1750-1850 CE) climates turned cold/wet. During the MCA, climatic conditions were relatively wet (not as wet as during the RWP and DACP) in the period of 900-1200 CE, but became warm and drier at the end of MCA (~1200-1300 CE). Hence, a warm (or cold) climate is not necessary accompanied with a wet (or dry) climate. As mentioned earlier, temperature change may shift toward the same direction over large regions, whereas precipitation may vary towards different conditions, wetter/drier, at different locations within the same region. In comparison with other paleorecords in the Altai region, the temperature conditions agreed well in the entire region (Agatova et al., 2012; Rudaya et al., 2016; Babich et al., 2023 and references therein). On the other hand, moderate wet climate during the MCA and dry climate during the LIA were also found in the Manzherok Lake record (about 110 km east of Zolotoe Lake) (Blyakharchuk et al., 2017, 2020). However, Lake Teletskoye (about 150 km east of Zolotoe Lake) did not show a dry LIA (Rudaya et al., 2016). Thus, moisture condition reconstructed from different lakes in the same region may be influenced by the geographic settings, sensitivity and sediment input. Of course, comparison of paleorecords in different locations requests robust chronology, high-resolution, and good understanding of different proxies. Hence, in order to obtain accurate regional climate conditions and their forcing factors over the past 2000 years, more high-resolution records with robust chronology are needed.

## 6. Conclusions

The $^{210}$Pb, $^{137}$Cs and AMS $^{14}$C datings of the 64-cm gravity core from Zolotoe Lake provide excellent chronology of the depositional history continuously spanning the past 1800 years. Comparison of paired AMS $^{14}$C dates of both acid-treated and acid-base-acid treated TOC samples from 20 horizons allows us to eliminate old carbon influence on some ABA treated samples due to uptake of dissolved $CO_2$ in the lake water.

In the Zolotoe Lake sediments, Sr/Ca and Mg/Ca values are not indicators of salinity because the source of Sr and Mg came from mainly carbonate minerals which were strongly affected by terrestrial input. AL Ca/K, on the other hand, is an indicator of salinity with higher ratio reflecting higher salinity due to $CaCO_3$ precipitation under higher pH and salinity. AL Al/Ti is a proxy of surface runoff with higher ratio reflecting higher surface runoff. AL Mn/Fe and Mn/Al are functions of redox conditions with higher ratio indicating more oxic conditions. AL U/Al is strongly positively correlated with AL Mn/Al due to scavenging with $MnO_2$ and $Al_2O_3$ precipitation, so that U/Al is not an indicator of redox conditions. AP development indicates cold and wet conditions compared to NAP, but NAP has also positive relationship with rainfall. Therefore, higher AP/NAP ratio reflects cold and wet climates, but lower AP/NAP ratio does not necessary reflect cold/dry or warm/dry conditions. Similarly, A/Cy and A/A ratios can also be influenced by hydroclimatic conditions, so that the relationship between these ratios and temperature is not necessarily positive. *Pediastrum* abundance in the Zolotoe Lake sediments has a positive relationship with lake salinity and nutrient concentration, but not MAT. Hence, using the above geochemical and pollen ratios in lake sediments requires detailed evaluation.

Combining the geochemical proxies (TOC-productivity, AL Ca/K-salinity, AL Al/Ti-surface runoff, AL Mn/Fe-redox, etc.) and pollen proxies (AP/NAP and A/Cy ratios) of the core 22-Al-03A, the climatic conditions in the study area over the past 1800 years can be estimated as follow: (1) during the RWP (~200-400 CE) relatively warm and wet conditions were prevailing, Zolotoe Lake was fresh, oxic with low productivity and high surface runoff; (2) cooler and wetter climate conditions occurred during the DACP (~450-800 CE) and resulted in the lowest salinity and low productivity in Zolotoe Lake. The lakes in the Volchikhinsky lake system might have been connected at that time forming a large lake; (3) warmer conditions probably occurred during the entire MCA interval (~900-1300 CE). Relatively wet conditions occurred during most of the MCA, but between 1200 and 1300 CE climate was drier. Climate was colder and drier during the early LIA (~1400-1750 CE). The large lake evolved into the modern Volchikhinsky lake system with separated lakes around 1600 CE. At the end of the LIA (1750-1850 CE) the climate was colder and wetter. Generally, wetter conditions in the study area existed between 1750 and 1950 CE. With the CWP (~1850-2020 CE), a warming trend is documented by both the instrumental record and the lake record. The Zolotoe Lake sediments document strong human impact since 1950 CE.

## Author's contribution

Corresponding author, H.-C. Li, initiated and supervised the study. He is in charge of interpretations of dating and geochemical analyses. The final manuscript was done by Li. Corresponding author, L. Frolova is in charge of coring, sample preparation and biological study. E. Mitwally performed on AMS 14C dating, XRD, SEM and initial manuscript draft. G. Nigamatzyanova conducted pollen analysis and wrote pollen related sections. T.-T. Shen obtained the results of EA measurements. V. Strakhovenko attended field work and performed SEM analysis. Andrei A. Andreev participated the pollen analysis and manuscript revise. S. Liou provides fund for publication.

## Declaration of competing interest

The authors declare that they have no known competing financial interests or personal relationships that could have appeared to influence the work reported in this paper.

## Acknowledgments

Thanks to the Instrumentation Center of National Taiwan University for support. This study was funded from the National Science and Technology Council of Taiwan (NSTC 111-2116-M-002-020, NSTC 112-2116-M-002-020 and NSTC 113-2116-M-002-003) to H-C Li. G. Nigamatzyanova and L. Frolova were supported with paleobiological analysis by the project FWZG-2025–0005. The conducting of expedition work and the study of mineralogy of bottom sediments were done on the state assignment of the Institute of Geology and Mineralogy SB RAS (No. 122041400193-7) with financial support from the Ministry of Science and Higher Education of the Russian Federation. We thank two anonymous reviewers for their constructive reviews. Special thanks to Dr. Patrick Rioual, editor for QSR, for the detailed editorial work.

## Appendix A. Supplementary data

Supplementary data to this article can be found online at https://doi.org/10.1016/j.quascirev.2026.109814.

## Data availability

All data and/or code is contained within the submission.

## References


Agatova, A.R., Nazarov, A.N., Nepop, R.K., Rodnight, H., 2012. Holocene glacier fluctuations and climate changes in the southeastern part of the Russian Altai (South Siberia) based on a radiocarbon chronology. Quat. Sci. Rev. 43, 74–93.

Andreev, A.A., Pierau, R., Kalugin, I.A., Daryin, A.V., Smolyaninova, L.G., Diekmann, B., 2007. Environmental changes in the Northern Altai during the last millennium documented in Lake Teletskoye pollen record. Quat. Res. 67, 394–399.

Andreenkov, S.N., 2021. State and collective farm system in the first half of the 1960s: development problems and antic-Crisis recommendations of scientific economists. Hist. Courier 18, 109–120. http://istkurier.ru/data/2021/ISTKURIER-2021-4-10.pdf (In Russian).

Appleby, P.G., 2000. Radiometric dating of sediment records in European mountain lakes. Limnology 59, 1–14.

Appleby, P.G., Oldfield, F., 1992. Application of lead-210 to sedimentation studies. In: Ivanovich, M., Harmon, R.S. (Eds.), Uranium-Series Disequilibria. Applications to Earth, Marine, and Environmental Sciences, second ed. Clarendon, Oxford. UK, pp. 731–778.

Aravena, R., Warner, B.G., Charman, D.J., Belyea, L.R., Mathur, S.P., Dinel, H., 1993. Carbon isotopic composition of deep carbon gases in an ombrogenous peatland, northwestern Ontario, Canada. Radiocarbon 35, 271–276.

Ascough, P., 2014. Peat ($^{14}$C). In: Rink, W., Thompson, J. (Eds.), Encyclopedia of Scientific Dating Methods. Springer, Dordrecht, pp. 1–8. https://doi.org/10.1007/978-94-007-6326-5_166-1.

Babich, V.V., Daryin, A.V., Rudaya, N.A., Markovich, T.I., 2023. Two millennia of climate history for the Russian Altai: integrated reconstruction from lake sediment data. Russ. Geol. Geophys. 64, 1217–1226. https://doi.org/10.2113/RGG20234585.

Barjaktarovic, L., Bendell-Young, L.I., 2002. Factors contributing to the salinity of lakes, Riske Creek region, south-central British Columbia, Canada. Appl. Geochem. 17, 605–619.

Baskaran, M., Bianchi, T.S., Filley, T.R., 2017. Inconsistencies between $^{14}$C and short-lived radionuclides-based sediment accumulation rates: effects of long-term remineralization. J. Environ. Radioact. 174, 10–16.

Bennett, K.D., Willis, K.J., 2001. Pollen. In: Smol, J.P., Birks, H.J.B., Last, W.M. (Eds.), Tracking Environmental Change Using Lake Sediments. Volume 3: Terrestrial, Algal, and Siliceous Indicators. Kluwer Academic, Dordrecht, pp. 5–32.

Bertrand, S., Tjallingii, R., Kylander, M.E., Wilhelm, B., Roberts, S.J., Arnaud, F., Brown, E., Bindler, R., 2024. Inorganic geochemistry of lake sediments: a review of analytical techniques and guidelines for data interpretation. Earth Sci. Rev. 249, 104639.

Bezrukova, E.V., Amosova, A.A., Chubarov, V.M., 2023. Geochemical records of the late glacial and Holocene paleoenvironmental changes from the Lake Kaskadnoe-1 sediments (East Sayan Mountains, South Siberia). Minerals 13, 449. https://doi.org/10.3390/min13030449.

Bezrukova, E.V., Reshetova, S.A., Shchetnikov, A.A., 2025. Reconstruction of the late Holocene environments in the northern Minusinsk Basin (South Siberia) based on the palynological analysis of Lake Shira sediments. J. Asian Earth Sci. 289, 106610.

Blaauw, M., Christen, J.A., 2011. Flexible paleoclimate age-depth models using an autoregressive gamma process. Bayesian Anal 6, 457–474.

Blyakharchuk, T., Eirikh, A., Mitrofanova, E., Li, H.-C., Kang, S.-C., 2017. High resolution palaeoecological records for climatic and environmental changes during the last 1350 years from Manzherok Lake, western foothills of the Altai Mountains, Russia. Quat. Int. 447, 59–74.

Blyakharchuk, T., Udachin, V., Li, H.-C., Kang, S.-C., 2020. AMS $^{14}$C dating problem and high-resolution geochemical record in Manzherok Lake sediment core from Siberia: climatic and environmental reconstruction for Northwest Altai over the past 1,500 years. Front. Earth Sci. 8, 206. https://doi.org/10.3389/feart.2020.00206.

Blyakharchuk, T., Wright, H.E., Borodavko, P.S., van der Knaap, W.O., Ammann, B., 2004. Late Glacial and Holocene vegetational changes on the Ulagan high-mountain plateau, Altai Mountains, southern Siberia. Palaeogeogr. Palaeoclimat. Palaeoecol. 209, 259–279.

Blyakharchuk, T., Wright, H.E., Borodavko, P.S., van der Knaap, W.O., Ammann, B., 2007. Late Glacial and Holocene vegetational history of the Altai Mountains (southwestern Tuva Republic, Siberia). Palaeogeogr. Palaeoclimatol. Palaeoecol. 245, 518–534.

Blyakharchuk, T., Wright, H.E., Borodavko, P.S., van der Knaap, W.O., Ammann, B., 2008. The role of pingos in the development of the Dzhangyskol lake-pingo complex, central Altai Mountains, southern Siberia. Palaeogeogr. Palaeoclimatol. Palaeoecol. 254, 404–420.

Bridgham, S.D., Richardson, C.J., 2003. Endogenous versus exogenous nutrient control over decomposition and mineralization in North Carolina peatlands. Biogeochemistry 65, 151–178. https://doi.org/10.2307/1469850.

Brock, F., Higham, T., Ditchfield, P., Ramsey, C.B., 2010. Current pretreatment methods for AMS radiocarbon dating at the Oxford radiocarbon accelerator unit. Radiocarbon 52, 103–112.

Broström, A., Nielsen, A.B., Gaillard, M.-J., Hjelle, K., Mazier, F., Binney, H., Bunting, M. J., Fyfe, R., Meltsov, V., Poska, A., Räsänen, S., Soepboer, W., von Stedingk, H., Suutari, H., Sugita, S., 2008. Pollen productivity estimates of key European plant taxa for quantitative reconstruction of past vegetation: a review. Veg. Hist. Archaeobotany 17, 461–478.

Bykov, N.I., Shigimaga, A.A., Rygalova, N.V., 2023. Response of the radial growth of woody plants in the West Siberian Plain and adjacent mountainous territories to the characteristics of the snow cover. Forests 14, 1690. https://doi.org/10.3390/f14081690.

Chanton, J.P., Bauer, J.E., Glaser, P.A., Siegel, D.I., Kelley, C.A., Tyler, S.C., Romanowicz, E.H., Lazrus, A., 1995. Radiocarbon evidence for the substrates supporting methane formation within northern Minnesota peatlands. Geochem. Cosmochim. Acta 59, 3663–3668.

Chappell, A., 1999. The limitations of using $^{137}$Cs for estimating soil redistribution in semi-arid environments. Geomorphology 29, 135–152.

Charman, D.I., Aravena, R.A., Warner, B.G., 1994. Carbon dynamics in a forested peatland in northeastern Ontario, Canada. J. Ecol. 82, 55–62.

Chen, B., Zhao, M., Yan, H., Yang, R., Li, H.-C., Hammond, D.E., 2021. Tracing source and transformation of carbon in an epikarst spring-pond system by dual carbon isotopes ($^{13}$C–$^{14}$C): evidence of dissolved $CO_2$ uptake as a carbon sink. J. Hydrol. 593, 125766.

Chen, F.H., Huang, X.Z., Zhang, J.W., Holmes, J.A., Chen, J.H., 2006. Humid little ice age in arid Central Asia documented by Bosten Lake, Xinjiang, China. Sci. China Earth Sci. 49, 1280–1290.

Chen, J.H., Chen, F.H., Feng, S., Huang, W., Liu, J.B., Zhou, A.F., 2015. Hydroclimatic changes in China and surroundings during the medieval climate anomaly and Little Ice Age: spatial patterns and possible mechanisms. Quat. Sci. Rev. 107, 98–111.

Chu, P.C., Li, H.-C., Fan, C.W., Chen, Y.-H., 2012. Speleothem evidence for temporal–spatial variation in the East Asian Summer Monsoon since the Medieval Warm Period". J. Quat. Sci. 27, 901–910.

Cook, G.T., Dugmore, A.J., Shore, J.S., 1998. The influence of pretreatment on humic acid yield and $^{14}$C age of *Carex* peat. Radiocarbon 40, 21–27.

Cui, Q.Y., Zhao, Y., Qin, F., Liang, C., Li, Q., Geng, R.W., 2019. Characteristics of the modern pollen assemblages from different vegetation zones in Northeast China: implications for pollen-based climate reconstruction. Sci. China Earth Sci. 62, 1564–1577. https://doi.org/10.1007/s11430-018-9386-9.

Dirin, D.A., Mardasova, E.V., Rygalov, E.V., 2017. Resources of recreation in the Kulunda steppe. Geogr Environ. Management Siberia 2, 11–33 (In Russian.).

Dong, S.P., Li, Z.L., Chen, Q.J., Wei, Z.Q., 2018. Total organic carbon and its environmental significance for the surface sediments in groundwater recharged lakes from the Badain Jaran Desert, Northwest China. J. Limnol. 77, 121–129. https://doi.org/10.4081/jlimnol.2017.1667.

El-Moslimany, A.P., 1990. Ecological significance of common nonarboreal pollen: examples from drylands of the Middle East. Rev. Palaeobot. Palynol. 64, 343–350.

Engstrom, D.R., Wright, H.E., 1984. Chemical stratigraphy of lake sediments as a record of environmental change. In: Haworth, E.Y., Lund, J.W.G. (Eds.), Lake Sediments and Environmental History. Leicester University Press, Leicester, pp. 11–67.

Fedorova, M.I., Manchenko, K.A., 2022. Methods and results of agricultural management in the Khrushchev Period – the experience of reconstructing everyday life (50-60s of the 20th century, based on materials from Western Siberia). Vestnik Omsk Univ. Series Histor. Studi. 9 (34), 96–106. https://doi.org/10.24147/2312-1300.2022 (in Russian).

Frolova, L.A., Nigmatullin, N.M., 2019. First record of *Phreatalona protzi* (Hartwig, 1900) (Branchiopoda: anomopoda) in a tundra lake in North-East European Russia. In: 19th International Multidisciplinary Scientific Geoconference SGEM, vol. 19, pp. 285–290, 5.1.

Frolova, L.A., Nigamatzyanova, G.R., Nigmatullin, N.M., Valieva, E.A., Frolova, A.A., 2022. A multi-proxy study of Holocene environmental and climate change in Pechora Delta. Limnol. Freshwater Biol. 4, 1421–1422. https://doi.org/10.31951/2658-3518-2022-A-4-1421.

Fægri, K., Iversen, J., 1989. Textbook of Pollen Analysis, fourth ed. John Wiley and Sons, p. 328.

Gaines, R.V., Skinner, H.C.W., Foord, E.E., Mason, B., Rosenzweig, A., 1997. Dana's new mineralogy. In: Am. Chem. Society. Wiley/VCH, New York, p. 1819.

Gaillard, M.-J., Sugita, S., Bunting, M.J., Middleton, R., Broström, A., Caseldine, C., Giesecke, T., Hellman, S.E.V., Hicks, S., Hjelle, K., Langdon, C., Nielsen, A.-B., Poska, A., von Stedingk, H., Veski, S., POLLANDCAL members, 2008. The use of modelling and simulation approach in reconstructing past landscapes from fossil pollen data: a review and results from the POLLANDCAL network. Veg. Hist. Archaeobotany 17, 419–443.

Gälman, V., Rydberg, J., Sjostedt, L.S., Bindler, R., Renberg, I., 2008. Carbon and nitrogen loss rates during aging of lake sediment: changes over 27 years studied in varved lake sediments. Limnol. Oceanogr. 53, 1076–1082.

Ganyushkin, D., Chistyakov, K., Derkach, E., Bantcev, D., Kunaeva, E., Terekhov, A., Rasputina, V., 2022. Glacier recession in the Altai Mountains after the LIA maximum. Remote Sens. 14, 1508. https://doi.org/10.3390/rs14061508.

Ge, Q.S., Liu, H.L., Ma, X., Zheng, J.Y., Hao, Z.X., 2017. Characteristics of temperature change in China over the last 2000 years and spatial patterns of dryness/wetness during cold and warm periods. Adv. Atmos. Sci. 34, 941–951.

Grimm, E.C., 1987. CONISS: a FORTRAN 77 program for stratigraphically constrained cluster analysis by the methods of incremental sum of squares. Comput. Geosci. 13, 13–15.

Grimm, E.C., 2004. TGView. Illinois State Museum, Research and Collections Center. Springfield.
Han, Q., Wang, L., Huang, L., Li, R., Li, P., Zhang, T., Zhou, Q., Chen, G., 2022. Anthropogenic control of coupled changes in organic and inorganic carbon burial in karst landscape: sediment evidence from two lakes of subtropical China. Ecol. Indic. 138, 108811.
Hardy, E.P., 1971. Fallout program quarterly summary report with appendix. U.S. Army Corp. of Eng. Doc. HASL-245 255.
Hausmann, S., Larocque-Tobler, I., Richard, P.J.H., Pienitz, R., St-Onge, G., Fye, F., 2011. Diatom-inferred wind activity at Lac du Sommet, southern Quebec, Canada: a multiproxy paleoclimate reconstruction based on diatoms, chironomids and pollen for the past 9500 years. Holocene 21, 925–938.
He, W.Y., You, L.H., Chen, M., Tuo, Y.C., Liao, N., Wang, H.W., Li, J., 2023. Varied sediment archive of Fe and Mn contents under changing reservoir mixing patterns, oxygenation regimes, and runoff inputs. Ecol. Indic. 147, 109967.
Helama, S., Jones, P.D., Briffa, K.R., 2017. Dark ages cold period: a literature review and directions for future research. Holocene 27, 095968361769389. https://doi.org/10.1177/0959683617693898.
Herzschuh, U., 2007. Reliability of pollen ratios for environmental reconstructions on the Tibetan Plateau. J. Biogeogr. 34, 1265–1273. https://doi.org/10.1111/j.1365-2699.2006.01680.x.
Hua, Q., Turnbull, L.C., Santos, G.M., Rakowski, A.Z., Ancapichún, S., De Pol-Holz, R., Hammer, S., Lehman, S.J., Levin, I., Miller, J.B., Palmer, J.G., Turney, C.S., 2022. Atmospheric radiocarbon for the period 1950-2019. Radiocarbon 64, 723–745.
Huang, X.Z., Huang, C., Xu, Y., Zheng, M., Ren, X.X., Chen, X.M., Hu, Y., Wang, T., Xiang, L.X., Zhang, J., Chen, F.H., 2023. Body size of fossil *Pediastrum* in lake sediments as an indicator of temperature variation. Palaeogeogr. Palaeoclimatol. Palaeoecol. 625, 111687.
Huang, X., Peng, W., Rudaya, N., Grimm, E.C., Chen, X., Cao, X., Zhang, J., Pan, X., Liu, S., Chen, Ch, Chen, F., 2018. Holocene vegetation and climate dynamics in the Altai Mountains and surrounding areas. Geophys. Res. Lett. 45, 6628–6636. https://doi.org/10.1029/2018GL078028.
Jiang, Q.F., Ji, J.F., Shen, J., Matsumoto, R.Y.O., Tong, G.B., Qain, P., Ren, X.M., Yan, D. Z., 2013. Holocene vegetational and climatic variation in westerly- dominated areas of Central Asia inferred from the Sayram Lake in northern Xinjiang. China. Sci. China. Earth Sci. 56, 339–353.
Kalugin, I., Darin, A., Rogozin, D., Tretyakov, G., 2013. Seasonal and centennial cycles of carbonate mineralisation during the past 2500 years from varved sediment in Lake Shira, South Siberia. Quat. Int. 290–291, 245–252.
Kalugin, I., Daryin, A., Smolyaninova, L., Andreev, A., Diekmann, B., Khlystov, O., 2007. 800-yr-long records of annual air temperature and precipitation over southern Siberia inferred from Teletskoye Lake sediments. Quat. Res. 67, 400–410.
Karachurina, S., Rudaya, N., Frolova, L., Kuzmina, O., Cao, X., Chepinoga, V., Stoof-Leichsenring, K., Biskaborn, B., Herzschuh, U., Nigmatullin, N., Vnukovskaya, Y., Grekov, I., Pestryakova, L., 2023. Terrestrial vegetation and lake aquatic community diversity under climate change during the mid–late Holocene in the Altai Mountains. Palaeogeogr. Palaeoclimatol. Palaeoecol. 623, 11623. https://doi.org/10.1016/j.palaeo.2023.111623.
Kasper, T., Frenzel, P., Haberzettl, T., Schwarz, A., Daut, G., Meschner, S., Wang, J., Zhu, L., Mäusbacher, R., 2013. Interplay between redox conditions and hydrological changes in sediments from Lake Nam Co (Tibetan Plateau) during the past 4000 cal BP inferred from geochemical and micropaleontological analyses. Palaeogeogr. Palaeoclimatol. Palaeoecol. 392, 261–271. https://doi.org/10.1016/j.palaeo.2013.09.027.
Kaushal, S., Binford, M.W., 1999. Relationship between C: n ratios of lake sediments, organic matter sources, and historical deforestation in Lake Pleasant, Massachusetts, USA. J. Paleolimnol. 22, 439–442.
Khazina, I.V., 2006. Reconstruction of the middle-late Holocene natural climatic conditions in the Ob' region near Novosibirsk (using palynological data from Lake Beloe sediments). Russ. Geol. Geophys. 47, 971–978.
Koinig, K.A., Shotyk, W., Lotter, A.F., Ohlendorf, C., Sturm, M., 2003. 9000 years of geochemical evolution of lithogenic major and trace elements in the sediment of an alpine lake - the role of climate, vegetation, and land-use history. J. Paleolimnol. 30, 307–320.
Lan, B., Zhang, D., Yang, Y., 2018. Lacustrine sediment chronology defined by $^{137}$Cs, $^{210}$Pb and $^{14}$C and the hydrological evolution of Lake Ailike during 1901-2013, northern Xinjiang, China. Catena 161, 104–112.
Lamb, H.H., 2011. Climate: Present, past and Future. Volume 2, Climatic History and the Future. Routledge, Abingdon, Oxon. ISBN 978-0-203-80430-8. OCLC 900419132.
Le Roux, G., Marshall, W.A., 2011. Constructing recent peat accumulation chronologies using atmospheric fall-out radionuclides. Mires Peat 7, 1–14.
Li, H.C., Bischoff, J.L., Ku, T.-L., Lund, S.P., Stott, L.D., 2000. Climate variability in east-central California during the past 1000 years reflected by high-resolution geochemical and isotopic records from Owens Lake sediments. Quat. Res. 54, 189–197.
Li, H.C., Bischoff, J.L., Ku, T.-L., Zhu, Z.-Y., 2004. Climate and hydrology of the last Interglaciation (MIS 5) in Owens Basin, California: isotopic and geochemical evidence from core OL-92. Quat. Sci. Rev. 23, 49–63.
Li, H.C., Chang, Y., Berelson, W.M., Zhao, M., Misra, S., Shen, T.T., 2022. Interannual variations of $D^{14}C_{TOC}$ and elemental contents in the laminated sediments of the Santa Barbara Basin during the past 200 years. Front. Mar. Sci. 9, 823793.
Li, H.C., Wang, J., Sun, J.J., Chou, C.Y., Li, H.K., Xia, Y.Y., Zhao, H.Y., Yang, Q.N., Kashyap, S., 2019. Study of Jinchuan Mire in NE China I: AMS $^{14}$C, $^{210}$Pb and $^{137}$Cs dating on peat cores. Quat. Inter. 528, 9–17.
Li, Q., Lu, H., Shen, C., Zhao, Y., Ge, Q., 2016a. Vegetation successions in response to Holocene climate changes in the central Tibetan Plateau. J. Arid Environ. 125, 136–144. https://doi.org/10.1016/j.jaridenv.2015.07.010.
Li, Z.L., Wang, N.A., Cheng, H.Y., Yu Li, Y., 2016b. Early-middle Holocene hydroclimate changes in the Asian monsoon margin of northwest China inferred from Huahai terminal lake records. J. Paleolimnol. 55, 289–302. https://doi.org/10.1007/s10933-016-9880-8.
Liang, C., Bo Yang, B., Cao, Y.C., Liu, K.Y., Wu, J., Hao, F., Han, Y., Han, W.L., 2024. Salinization mechanism of lakes and controls on organic matter enrichment: from present to deep-time records. Earth Sci. Rev. 251, 104720.
Liu, X.Q., Herzschuh, U., Shen, J., Jiang, Q., Xiao, X., 2008. Holocene environmental and climatic changes inferred from Wulungu Lake in northern Xinjiang. China. Quat. Res. 70, 412–425.
Lone, A., Fousiya, A.A., Shah, R., Achyuthan, H., 2018. Reconstruction of paleoclimate and environmental fluctuations since the early Holocene period using organic matter and C:N proxy records: a Review. J. Geol. Soc. India 91, 209–214.
Lu, L.-L., Jiao, B.-H., Qin, F., Xie, G., Lu, K.-Q., Li, J.-F., Sun, B., Li, M., Ferguson, D.K., Gao, T.-G., Yao, Y.-F., Wang, Y.-F., 2022. *Artemisia* pollen dataset for exploring the potential ecological indicators in deep time. Earth Syst. Sci. Data 14, 3961–3995. https://doi.org/10.5194/essd-14-3961-2022.
Lü, X., Paudayal, K.N., Uhl, D., Zhu, L.P., Yao, T.D., Mosbrugger, V., 2020. Phenology and climatic regime inferred from airborne pollen on the northern slope of the Qomolangma (Everest) region. J. Geophys. Res., [Atmos.] 125. https://doi.org/10.1029/2020JD033405 e2020JD033405.
Ma, Q.F., Zhu, L.P., Ju, J.T., Wang, J.B., Wang, Y., Huang, L., Haberzett, T., 2024. A modern pollen dataset from lake surface sediments on the central and western Tibetan Plateau. Earth Syst. Sci. Data 16, 311–320. https://doi.org/10.5194/essd-16-311-2024.
Mann, M.E., Zhang, Z.H., Rutherford, S., Bradley, R.S., Hughes, M.K., Shindell, D., Ammann, C., Faluvegi, G., Ni, F., 2009. Global signatures and dynamical origins of the Little Ice Age and Medieval climate Anomaly. Science 326, 1256–1260.
Meyers, P.A., Ishiwatari, R., 1993. Lacustrine organic geochemistry-an overview of indicators of organic matter sources and diagenesis in lake sediments. Org. Geochem. 20, 867–900.
Michel, H., Chitty, D., Barci-Funel, G., Ardisson, G., Appleby, P.G., Haworth, E., 2002. Comparison of $^{210}$Pb chronology with $^{238,239-240}$Pu, $^{241}$Am and $^{137}$Cs sedimentary record capacity in a lake system. In: Fichez, R., Fernandez, J.M. (Eds.), Environmental Changes and Radioactive Tracers. Springer International Publishing, Heidelberg, pp. 213–222.
Misra, S., Kashyap, S., Chou, C.Y., Chang, T., Li, H.C., Ning, X., Sun, J.J., Wang, J., Zhao, M., 2024. The influence of plant species and pretreatment on the $^{14}$C age of Carex-dominated peat plants of a peat core from Jinchuan Mire, NE China. Radiocarbon 66 (5), 937–957. https://doi.org/10.1017/RDC.2023.112.
Misra, S., Kuzina, D., Shen, T.-T., Chou, C.-Y., Yusupova, A., Krylov, P., Nurgaliev, D., Li, H.-C., 2025. Accessing old carbon influence on TOC $^{14}$C age and environmental change from the recent sediments in Lake Shira, Russia. Radiocarbon 1–24. https://doi.org/10.1017/RDC.2024.129.
Nazarova, L., Krasheninnikov, A.B., Frolova, L.A., Palagushkina, O.V., Golovatyuk, L.V., Syrykh, L.S., Biskaborn, B.K., Fuchs, F.G.E., Gavrilo, M.V., 2025. Evolution of the hydrobiological communities of a coastal lake in the Novaya Zemlya Archipelago (Southern Island, Arctic Russia) in relation to climate change following the end of the Little Ice Age. Water 17, 1868.
Neukom, R., Steiger, N., Gómez-Navarro, J.J., Wang, J.H., Werner, J.P., 2019. No evidence for globally coherent warm and cold periods over the preindustrial common era. Nature 571, 550–554. https://doi.org/10.1038/s41586-019-1401-2.
Nigamatzyanova, G.R., Nigmatullin, N.M., Frolova, L.A., 2024. Pollen analysis in reconstruction of paleo vegetation on the southwestern part of the Yamal Peninsula. Limnol. Freshwater Biol. 4, 757–760. https://doi.org/10.31951/2658-3518-2024-A-4-757.
Nigmatullin, N.M., Nigamatzyanova, G.R., Valieva, E.A., Tumanov, O.N., Frolova, L.A., 2022. Subfossil records of the Cladocera from tundra lake in Yamal Peninsula. Limnol. Freshw. Biol. 4, 1515–1516. https://doi.org/10.31951/2658-3518-2022-A-4-1515.
Perdue, E.M., Koprivnjak, J.F., 2007. Using the C/N ratio to estimate terrigenous inputs of organic matter to aquatic environments, Estuarine. CoastalShelf Sci. 73, 65–72.
Qin, F., Zhao, Y., Li, Q., Cai, M.T., 2015. Modern pollen assemblages from surface lake sediments in northwestern China and their importance as indicators of vegetation and climate. Sci. China Earth Sci. 58, 1643–1655. https://doi.org/10.1007/s11430-015-5111-9.
Reimer, P.J., Austin, W.E.N., Bard, E., Bayliss, A., Blackwell, P.G., Bronk, R.C., Butzin, M., Cheng, H., Edwards, R.L., Friedrich, M., Grootes, P.M., Guilderson, T.P., Hajdas, I., Heaton, T.J., Hogg, A.G., Hughen, K.A., Kromer, B., Manning, S.W., Muscheler, R., Palmer, J.G., Pearson, C., van der Plicht, J., Reimer, R.W., Richards, D.A., Scott, E.M., Southon, J.R., Turney, C.S.M., Wacker, L., Adolphi, F., Capano, M., Fahrni, S.M., Fogtmann-Schulz, A., Friedrich, R., Kudsk, S., Miyake, F., Olsen, J., Reinig, F., Sakamoto, M., Sookdeo, A., Talamo, S., 2020. The INTCAL20 northern hemisphere radiocarbon age calibration curve (0-55 cal k BP). Radiocarbon 62, 1–33. https://doi.org/10.1017/RDC.2020.41.
Ritchie, J.C., McHenry, J.R., Gill, A.C., 1973. Dating recent reservoir sediments. Limnol. Oceanogr. 18, 254–263.
Rowan, D.J., Kalff, J., Rasmussen, J.B., 1992. Profundal sediment organic content and physical character do not reflect lake trophic status, but rather reflect inorganic sedimentation and exposure. Can. J. Fish. Aquat. Sci. 49, 1431–1438.
Rudaya, N., Li, H.-C., 2013. A new approach for reconstruction of the Holocene climate in the Mongolian Altai: the high-resolution $^{13}$C records of TOC and pollen complexes in Hoton-Nur Lake sediments. J. Asian Earth Sci. 69, 185–195.

Rudaya, N., Nazarova, L., Nurgaliev, D., Palagushkina, O., Papin, D., Frolova, L., 2012. Mid-late Holocene environmental history of Kulunda, southern West Siberia: vegetation, climate and humans. Quat. Sci. Rev. 48, 32–42. https://doi.org/10.1016/j.quascirev.2012.06.002.

Rudaya, N., Nazarova, L., Novenko, E., Andreev, A., Kalugin, I., Daryin, A., Babich, V., Li, H.-C., Shilov, P., 2016. Quantitative reconstructions of mid- to late Holocene climate and vegetation in the north-eastern Altai Mountains recorded in Lake Teletskoye. Global Planet. Change 141, 12–24.

Ryabogina, N.E., Afonin, A.S., Ivanov, S.N., Li, H.-C., Kalinin, P.A., Udaltsov, S.N., Nikolaenko, S.A., 2019. Holocene paleoenvironmental changes reflected in peat and lake sediment records of Western Siberia: geochemical and plant macrofossil proxies. Quat. Int. 528, 73–87.

Saulnier-Talbot, É., Pienitz, R., Stafford, J.T., 2009. Establishing Holocene sediment core chronologies for northern Ungava lakes, Canada, using humic acids (AMS $^{14}$C) and $^{210}$Pb. Quat. Geochronol. 4, 278–287.

Scholtysik, G., Goldhammer, T., Arz, H.W., Moros, M., Littke, R., Hupfer, M., 2022. Geochemical focusing and burial of sedimentary iron, manganese, and phosphorus during lake eutrophication. Limnol. Oceanogr. 67, 768–783.

Shen, T.-T., Li, H.-C., Qiu, R., 2024. A homemade semiautomatic graphitization device for AMS $^{14}$C dating at NTUAMS LAB. Radiocarbon 66, 1345–1353.

Shi, F., Sun, C., Guion, A., Yin, Q.Z., Zhao, S., Liu, T., Guo, Z.T., 2021. Roman warm period and late Antique little ice age in an Earth system model large ensemble. J. Geophys. Res. Atmos. 127. https://doi.org/10.1029/2021JD035832 e2021JD035832.

Shichi, K., Goebel, T., Izuho, M., Kashiwaya, K., 2023. Climate amelioration, abrupt vegetation recovery, and the dispersal of *Homo sapiens* in Baikal Siberia. Sci. Adv. 9, eadi0189.

Shore, J.S., Bartley, D.D., Harkness, D.D., 1995. Problems encountered with the $^{14}$C dating of peat. Quat. Sci. Rev. 14, 373–383.

Skaldina, O.V., Slizh, E.A., 2018. The Great Red Book: the Most Complete List of Rare and Endangered Species of Animals in Russia, p. 478 (in Russian).

Smol, J.P., Cumming, B.F., 2000. Tracking long-term changes in climate using algal indicators in lake sediments. J. Phycol. 36, 986–1011.

Smrzka, D., Zwicker, J., Bach, W., Feng, D., Himmler, T., Chen, D., Peckmann, J., 2019. The behavior of trace elements in seawater, sedimentary pore water, and their incorporation into carbonate minerals: a review. Facies 65, 41. https://doi.org/10.1007/s10347-019-0581-4.

Solomina, O.N., Bradley, R.S., Jomelli, V., Geirsdottir, A., Kaufman, D.S., Koch, J., McKay, N.P., Masiokas, M., Miller, G., Nesje, A., Nicolussi, K., Owen, L.A., Putnam, A.E., Wanner, H., Wiles, G., Yang, B., 2016. Glacier fluctuations during the past 2000 years. Quat. Sci. Rev. 149, 61–90.

Stockmarr, J., 1971. Tablets with spores used in absolute pollen analysis. Pollen Spores 13, 615–621.

Swanson, G., Langman, J.B., Child, A.W., Wilhelm, F.M., Moberly, J.G., 2023. Iron and manganese oxidation states, bonding environments, and mobility in the mining-impacted sediments of Coeurd'Alene Lake, Idaho: core experiments. Hydrology 10, 23. https://doi.org/10.3390/hydrology10010023.

Tang, H.Y., Tan, M.L., Feng, Z.Q., Samat, N., Zhang, F., 2025. Solar radiation modification impact on precipitation and temperature extremes in Hunan, China. J. Hydrol. Region. Stud. 61, 102728.

Turner, F., Zhu, L.P., Lü, X.M., Peng, P., Ma, Q.F., Wang, J.B., Hou, J.Z., Lin, Q.Q., Yang, R.M., Frenzel, P., 2016. *Pediastrum* sensu lato (Chlorophyceae) assemblages from surface sediments of lakes and ponds on the Tibetan Plateau. Hydrobiologia 771 (1), 101–118.

van Vugt, L., Garces-Pastor, S., Gobet, E., Brechbühl, S., Knetge, A., Lammers, Y., Stengele, K., Alsos, I.G., Tinner, W., Schworer, C., 2022. Pollen, macrofossils and *sed*aDNA reveal climate and land use impacts on Holocene mountain vegetation of the Lepontine Alps, Italy. Quat. Sci. Rev. 296, 107749.

Wang, W., Feng, Z.D., 2013. Holocene moisture evolution across the Mongolian Plateau and the surrounding areas, a synthesis of climatic records. Earth Sci. Rev. 122, 38–57.

Welc, F., Nitychoruk, J., Marks, L., Binka, K., Rogóz-Matyszczak, A., Obremska, M., Zalat, A., 2021. 2400 years of climate and human-induced environmental change recorded in sediments of Lake Młynek in northern Poland. Clim. Past 17, 1181–1198. https://doi.org/10.5194/cp-17-1181-2021.

Wuebbles, D.J., Fahey, D.W., Hibbard, K.A., 2017. Climate science special report: fourth national climate assessment, volume I. U.S. Glob. Change Res. Prog. https://doi.org/10.7930/J0J964J6.

Xiang, L.X., Huang, X.Z.X.Z., Huang, C., Chen, X.M., Wang, H.P., Chen, J.H., Hu, Y., Sun, M.J., Xiao, Y.L., 2021. *Pediastrum* (Chlorophyceae) assemblages in surface lake sediments in China and western Mongolia and their environmental significance. Rev. Palaeobot. Palynol. 289, 104396.

Yang, B., Ljung, K., Nielsen, A.B., Fahlgren, E., Hammarlund, D., 2021. Impacts of long-term land use on terrestrial organic matter input to lakes based on lignin phenols in sediment records from a Swedish forest lake. Sci. Total Environ. 774, 145517.

Zhang, C.J., Zhang, L., Zhang, W.Y., Tao, Y.H., Liu, Y., Wan, X.L., Zhang, Z., Safarov, K., 2020a. Lake-level oscillation based on sediment strata and geochemical proxies since 11,000 year from Tengger Nuur, Inner Mongolia, China. Front. Earth Sci. 8, 314. https://doi.org/10.3389/feart.2020.00314.

Zhang, D., Chen, X., Li, Y., Zhang, S., 2020b. Holocene vegetation dynamics and associated climate changes in the Altai Mountains of the arid Central Asia. Palaeogeogr. Palaeoclimatol. Palaeoecol. 550, 1–8.

Zhang, D.L., Feng, Z.D., 2018. Holocene climate variations in the Altai Mountains and the surrounding areas: a synthesis of pollen records. Earth Sci. Rev. 185, 847–869.

Zhang, Y., Meyers, P.A., Liu, X., Wang, G., Ma, X., Li, X., Yuan, Y., Wen, B., 2016. Holocene climate changes in the central Asia mountain region inferred from a peat sequence from the Altai Mountains, Xinjiang, northwestern China. Quat. Sci. Rev. 152, 19–30.

Zhou, W., Chui, Y., Yang, L., Cheng, P., Chen, N., Ming, G., Hu, Y., Li, W., Lu, X., 2021. $^{14}$C geochronology and radiocarbon reservoir effect of reviewed lakes study in China. Radiocarbon 64, 833–844.